An Ab-initio Computational Investigation into the Properties of potentially Ultra-Hard Metal Oxynitrides

By

Fiki Martin Mmethi

A dissertation submitted to the Faculty of Science,

University of the Witwatersrand,

In fulfillment of the requirements for the degree

of Master of Science.

Department of Physics,

University of the Witwatersrand,

Johannesburg,

South Africa.

Declaration

I declare that this dissertation is my own work. It is being submitted for the degree of Master of Science in the University of the Witwatersrand, Johannesburg. It has not been submitted before for any degree or examination in any other university.

…….FIKI MARTIN MMETHI

……..day of …….2008

Dedication

To my parents: Malose Sinah and the late Kwena Nicodimus Mmethi (1940 - 2007)

To my brothers: Kgabo William, Choene Peter, Tlou Matthews, Nare Leonard, and the late Noko Jack (my younger brother)

To my younger sister Phuti Phillipine

!!!!! Basitoa ka moka!!!!

Acknowledgement

Firstly I would like to thank Professor J. E. Lowther for giving me an opportunity to work with him. I really appreciate him for his advice, guidance and courageous support throughout my research work. I really enjoyed working with him.

I would also like to acknowledge my family for their patience and support during the tough times of my studies.

Sincere thanks to my friends (Selepe Martin, Mokoka Christopher Dennis, Kgole Asaph, Molele Samuel, Warra Jack Mmethi, Motswala Tshidi Thomas Sehona, and Selepe Mokibelo Philly) for after-hours. Their support, patience and friendly atmosphere helped me a lot in my research and life here at Johannesburg.

I greatly acknowledge my officemate Thabo Letsoalo, Mahlaga Molepo and Onyekwelu Okeke for their valuable contribution in this work. My sincere thanks also go to all my teachers from Ngoako primary to Seripa high School especially my Physical Science and Mathematics teachers Mr. Matlapu, Mr Masipa and Mr Sathekge (Principal). My gratitude is also expressed to all my University lectures.

Lastly, the financial support received from DST-NRF CENTRE OF EXCELLENCE IN STRONG MATERIALS and the University of the Witwatersrand is greatly acknowledged.

!!!!!!!!!! Ka Sepedi bare: Lehlaku le lefsa le ema ka le letala. !!!!!!!!

Abstract

Ab-initio calculation are undertaken to compare some phases of several metal oxynitrides namely: titanium (TiON), tantalum (TaON), niobium (NbON), and tungsten (WON). The crystal structures considered follow that found in zirconia (ZrO_2) namely monoclinic, cubic, tetragonal, and orthorhombic. Bulk moduli and relative energies are obtained for each of the structures. In general it is found that quite high hydrostatic pressures are needed for synthesis of these materials although each of them exhibit quite significant compressibility. Diamonds is a super hard material useful for many applications but it's expensive to manufacture and its applications is somehow limited. The analyses here were carried out to examine properties of the oxynitride phases and estimate the pressure needed for a synthesis of such phases. These alloys are expected to have variety of interesting and novel future industrial application in many fields.

Table of Contents

List of figures

List of Tables

1 Introduction

The dream of synthesizing new superhard materials is one of the central challenges to modern day materials science. Materials with extreme hardness approaching or perhaps surpassing that of diamond are in great demand for technological and industrial usage. Within the last decade technological and the industrial development has been increasingly dependent on advanced materials. There is clear indication that this trend will continue to increase. Diamond is the hardest know material with many outstanding applications, but it has some drawbacks. It is not suitable for cutting and polishing ferrous alloys since it tends to react and form iron carbide. Cubic boron nitride the second hardest material is used to cut steel because iron borides and nitrides are much less stable. However, cubic boron nitride have been synthesized at high pressure of ≥ 5 GPa and temperatures $\geq 1600^{\circ}$C, making it expensive. Therefore, there is a need for synthetic materials that can be used in place of diamond and cubic boron nitride. The search for novel solid state materials with advanced properties was dominated by investigation on binary metal carbides, nitrides, and oxides for decades. In recent years there is interest to combine these binary compounds in form of metal oxynitrides and carbon nitrides. The main goal is to combine the properties of binary components and show that the mixed ternary compounds can have new chemical and physical properties and thus allow for exciting application. For example, technological use of oxynitrides

has first been identified in the fields of ionic conductivity and also bifunctional catalysis [1].

Several phases of metal oxynitrides (TiON, TaON, NbON and WON) are explored in this work, since they are expected to have variety of interesting and novel future industrial application. Emphasis is placed on the relative energies of different phases and their stability. Metal oxynitrides may naively be considered as being simple combinations of oxides and nitrides but some of them exhibit fascinating chemical and physical properties which are not seen for oxide and nitrides alone, and therefore oxynitrides allow for new application. Ti compounds also have many outstanding industrial application and notably, cotunnite TiO_2 has recently been reported to be the hardest known oxide. For that reason, theoretical calculations are ideally suited to examine the structural properties of TiON. Recently TaON is one of the most investigated transition metal oxynitrides, but has not much consideration as potentially hard material. TaON is candidate for applications that include photocatalyst, pigment and for use of the electronic industry [2-5]. So the theoretical calculations are important for understanding the structural properties (TaON). For comparison the properties of NbON have been investigated, since NbON adopt the same structure as TaON. So far one of the transition metal oxynitrides WON is expected to have some interesting properties, but has not received much attention as hard materials.

In this thesis we use ab-initio quantum mechanical molecular dynamic (MD) simulations employing the projector-augmented wave (PAW) method in the Vienna Ab-initio Simulation Package (VASP) code. The PAW method introduced by Blochl [6] is built on projector functions that allow the complicated wave functions to be mapped onto 'pseudo' wave functions, which are easier to treat. With this method, we model the core electrons taking the difference between the 'true' wave functions and a pseudo wave function obtained and neglecting the core electrons. The Schrödinger equation is expressed as:

$$\tau^{*} H \tau\tilde{\varphi} = E \tau\tau^{*}\tilde{\varphi} \qquad 1.1$$

Where $\tilde{\varphi}$ is the pseudowave function and τ is the operator of transformation that connects the exact wave functions (φ) and the pseudowave function $(\tilde{\varphi})$. In density functional theory (DFT), we solve the Schrödinger equation to determine the 'pseudo' wave functions. Projectors then enable us to obtain the exact density (whenever the basis set expansion is complete). The PAW method has extensively proven its high performance for studying molecules, surfaces and solids. We therefore used these pseudopotentials to perform our calculations. Details of PAW method are explained in section 4.3.3.

So far theoretical studies about the transition metal oxynitrides are quite limited. The ab-initio calculations we are using are based upon the local density approximation (LDA) and the generalized gradient approximation (GGA) under the density functional

theory (DFT) which will be discussed in chapter 4. Both LDA and GGA have proved to be reliable and computational tractable tools in condensed matter physics for treating the electron exchange correlation and studying new materials. Condensed matter physics and materials are concerned fundamentally with understanding and exploiting the properties of interacting electrons and atomic nuclear [7]. The advantage of ab-initio calculations is that they provide unbiased microscopic information that is not available from other sources. This gives important understanding of complex phenomena where experiments and simple models aren't sufficient. Over the past years, application of DFT has become the most effective method for the calculation of ground state structural and electronic properties of molecules and solids [8]. It is safe to say that without DFT, the impact of computational materials science would have been substantially less significant.

1.1 Synopsis

This thesis is arranged as follows: It contains an introductory chapter which introduces the concepts of this thesis. In chapter 2 and 3 the theoretical background for superhard materials and the concepts of hardness has been reviewed. Chapter 4 describes the theoretical background and presents the theoretical technique. Chapter 5 and 6 considered the background of metal oxynitrides and the results (are discussed). Finally chapter 7 summarizes and concludes the overview and the thesis.

2 Superhard Materials

Superhard materials are of the extreme importance in modern science and technology due to their superior properties [9-11]. From a fundamental point of view such materials may be defined as material with microhardness exceeding 4000 Kg mm^{-2} on the knoop scales [12]. Generally superhard materials are composed of light elements such as carbon, boron, oxygen and nitrogen [13, 14]. Li and Be are elements in the same period as B, C, N, and O but cannot form superhard structure as they have too few electrons to form strong bonding between atoms. Diamond is still the undisputed hardness substance. It is the hardest known substance, with a high thermal conductivity, high melting temperature, high elastic constant and it is a wide-gap semiconductor with a band gap (5.5 eV) [15,16]. Due to its superior hardness, diamond has been used to cut and polish all types of gem-grade stones. Beside its usefulness as an abrasive, other uses include wear and corrosion resistant coatings, heat sinks in electronic components, infrared windows in heat detectors, surgical blades, glass cutting and engraving tools, wire drawing dies, metal cutting tools and drill bits. Although diamond has much outstanding applicability, there are limitations to it. For example, diamond is not effective for cutting ferrous metals, including steel, because of a chemical reaction that produces iron carbide. Therefore, there is a need to look for materials that can be used

in place of diamond. Cubic boron nitride with a structure analogous to that of diamond can be used to cut ferrous metals because iron borides and nitrides are much stable.

Diamonds is hard because the chemical bond between each carbon that makes up diamond is extremely strong and another reason is that the atoms are connected to four others, forming a very regular cubic network. Carbon's bond strength and small size enable it to form a dense stronger mesh of atomic bonds than in any other material. Other carbon based materials have shorter and stringer carbon bonds, but not in three dimensions. For example, the trigonal sp^2 bonds in graphite form sheets with shorter and stronger carbon bonds, but only weak van der Waals interactions hold the sheets together, allowing layers of graphite to cleave readily. A three dimensional network composed of short, strong bonds is thus critical for hardness. The hardness of diamond comes from the stiffness of its tetravalent carbon bonds, which are also the basis of the widely used diamond–like coating. However, natural diamond is rare and its industrial production quite limited. For this reason, much experimental and theoretical work has been devoted to studying novel potential candidates for low compressibility materials [17].

A general theoretical approach to study hardness in any of its definitions is difficult, if not impossible, to perform. Traditionally, it has been linked to a large bulk modulus (B) but it has also been shown to correlate better with the shear modulus (G) of the

material; diamond is the leading system in both cases, with B = 443 GPa and G = 535 GPa, respectively [18]. In fact superhard materials usually meet the following conditions: of shorter bond length, higher electronic density or bond density, and greater degree of covalent bonding [11]. Strong covalent compounds formed by light elements, such as polymorph of C_3N_4 [19], B_6O [20], and C-B_2N [21] and partially covalent heavy transition metal boride, carbide, nitride and oxide such as RuO_2 [22], ZrO_2, HfO_2 and TiO_2 [23] are powerful candidates for superhard materials.

The cubic phase of boron nitride (BN) is known as the second hardest material after diamond with B =367 GPa [12] and G =405 GPa, whose structure is derived from that of diamond with half the carbon atoms being replaced by boron and the other half by nitrogen atoms. Cubic BN have been synthesized at high pressure of $\geq$ 5 GPa and temperatures $\geq$ 1600˚C, and does not exist in nature. It has several outstanding qualities, such as hardness surpassed only by diamond, high thermal temperature, low chemical reactivity, high electrical resistance, and low density. The combination of these properties makes cubic boron nitride more suitable as an engineering material than diamond for many applications, especially for wear. For example, diamond cannot be used to machine steels, particularly hardened steels, because carbon dissolves into steel at high tool tip temperature. Cubic boron nitride, in comparison, has a very low affinity to steel, therefore making it a promising candidate for machining. However, its synthesis is more difficult, and it has not been possible to prepare large crystals.

Therefore industry is looking for alternative materials that will need to be much harder than present ceramics (Si_3N_4, Al_2O_3, TiC).

A more elaborate material with a cubic structure and having potentially hard characteristics is the spinel structure (space group $Fd\bar{3}m$, Z = 8) where, in contrast to previously considered materials, the cation to anion ratio is 3:4 [24]. A high pressure phase of SiO_2-stishovite (33 GPa) is the hardest material known, after diamond and c-BN [25], but has not been stabilized for technological use. The hardness of γ-Si_3N_4 approaches that of SiO_2-stishovite but is significantly below that of diamond and c-BN. The property making γ-Si_3N_4 to an outstanding material is its excellent thermal (meta)stability in air superior to that of other superhard material such as diamond, c-BN, c-BC_2N, SiO_2-stishovite, and B_4C or B_6O[24]. High pressure cotunnite structured phase of titanium dioxide has been identified as the hardest known oxide synthesized to date with B = 431 GPa and hardness of 38 GPa [26].

The origin of superhardness in group IV nitride spinels results mainly from tetrahedron atoms rather than from sixfold coordination atoms. Other nitride polymorphs, experimentally detected and theoretically proposed, have also been studied. It is clear that increase of coordination cannot always results in increasing hardness [10]. Nitride spinels with hard characteristics have been found in both normal and the inversed form but the hardest found to date, namely γ-Si_3N_4 does not display such subtle differences

[24]. In many of the structural measurements carried out for γ-Si_3N_4 and γ-Ge_3N_4, the bulk properties including the elastic moduli and hardness are the natural outcome [27].

Recently Gregoryanz *et al* [28] reported the synthesis of platinum nitride (PtN). It was found that the compound has remarkably high bulk modulus of 372 GPa. This B is comparable to 382 GPa of superhard cubic zb-structure of BN [29]. Thus PtN is the first noble metal nitride experimentally identified to be superhard material. Theoretically Patil *et al* [30] reported the B of zb-PtN to be 230 GPa which is lower compared to the experimental value of 372 GPa [28]. Other theoretical investigations [31] have applied different density functional method to calculate bulk moduli and the lattice constant of various forms of PtN. These show that the structure and the bulk modulus of zb-PtN are not consistent with experiments.

The search of superhard materials is linked to the study of low compressibility solids, which have high values of bulk modulus or shear modulus. Transition metal containing compounds have large cohesive energies and high bulk modulus, associated with the distribution of their valence electrons between bonding and anti-bonding states within the partly filled electronic bands. Cynn *et al* [32] has found that osmium (Os), which is the heaviest elemental crystals, is less compressible to diamond with bulk modulus of 462 GPa exceeding that of diamond B = 443 GPa. However its hardness is quite low. Hebbache *et al* [33] synthesized OsB_2, found this material to be extremely hard; it is

also a low compressibility material with B = 342 GPa. Ab-initio calculations showed that is due to formation of covalent bonds between boron atoms [33]. Several studies of c-BC_2N have also been reported [34-36]. Komatsu *et al* [34] used shock wave compression to get c-BC_2N with B = 401 GPa, which is larger than of c-BN (~369 - 400 GPa). Solozhenko *et al* [35] synthesized c-BC_2N from graphite BC_2N at pressure above 18 GPa and temperatures higher than 2200 K. He found the bulk modulus of c-BC_2N to be B = 282 GPa which is one of the highest bulk modulus of solids and is exceeded only by diamond and indicates that the synthesized phase of BC_2N is only slightly less hard than diamond. Theoretically Chen [37] found the B of c-BC_2N to be 419 GPa, which is consistent with experimental findings, but in contrast with a recent theoretical study, which claimed that the c-BC_2N is less hard than diamond [38]. One of the new superhard materials formed at high pressure and temperature include dense partly polymerized forms of fullerite (C_{60}, C_{70} solids) [39]. Boron suboxide (B_6O_{1-x}) is another superhard material (H_v = 32-38 GPa) with a structure containing icosahedra grouping of boron atoms [40].

3 Hardness and its concepts

Hardness (H) is usually defined as the resistance of a material to deformations. Resistance to plastic deformation depends primarily on dislocation mobility. The hardness of a material may be written as: [41]

$$H = H_{\text{int}} + H_{ext} \qquad 3.1$$

Where H_{int} and H_{ext} are the intrinsic and extrinsic contributions to the hardness respectively. H_{int} is due to the nature of the bonding structure of the material, while H_{ext} is a result of the defective nature in the materials, and includes solid solution, precipitation, grain boundary, work hardening etc. Hence hardness strongly depends on the microstructure of the films. Hardness also depends on various other parameters: temperature, pressure, porosity, impurities, and dislocation movement. It also correlates to various physical properties such as ionicity, melting point, band gap, cohesive energy, etc., can therefore be then studied indirectly [42]. Probably the major requirements of a hard material are approximately isotropy – the bonding symmetry probably needs to be cubic, the valance electron density should be as large as possible and bonding type must be covalent. In addition dislocation mobilities in the material need to be as small as possible [43]. Covalent materials are much better candidates for

high hardness than ionic compounds because localized electrostatic interactions are omnidirectional and yield low bond-bending force constants, which results in low shear moduli. The ratio of bond-bending to bond-stretching force constants decreases linearly from about 0.3 for covalent material to essential zero for a purely ionic compound [44, 39]. Covalent bonds are strongest among other types of bonds, they are so strong in such a way that they disallow atom from sliding against one another.

There is no one to one correspondence between hardness and other properties. Hardness is different from bulk modulus or shear [39]. It is now accepted that the hardness of perfect crystals is mainly intrinsic and that of nanocrystalline and polycrystalline is extrinsic. Recently the works for hunting new superhard materials indicate that synthesis of materials with intrinsic hardness exceeding that of diamond is great challenge to science [45]. Materials with extrinsic hardness exceeding that of diamond were investigated frequently [46]. The goal of hardness design is to use knowledge of elastic stiffness and plastic resistance to propose a superhard material. Bulk modulus measure the resistance of a solid to volume change and is the simplest measure of elastic stiffness. The bulk modulus B is the reciprocal of compressibility. It expresses the material resistant to hydrostatic pressure [47]. Low compressibility materials are often superhard. Compressibility is an important physical property of a material, providing useful information about material strength, chemical bonding and electronic structure. Strong bonded materials have short interatomic forces, leading to high bulk

moduli [32]. The bulk modulus has been considered for along time as the best guide in search of high hardness materials. It is used because is cheaper to calculate from the practical usage of computer time. Materials with bulk modulus greater than a value of approximately 250 GPa can be considered as falling within a region where they could have a potential superhard character [13]. Even if there is a correlation between the hardness values and the bulk moduli for particular classes of substances [12], there are limitations when using bulk modulus for predicting hardness. For example, the bulk modulus of corundum exceeds that of B_6O, yet its hardness is significantly less [39]. Even though materials with bulk modulus higher than that of diamond have been predicted, none of them have higher shear modulus or hardness [14]. The fact that the bulk modulus of Os is comparable with that of diamond does not mean that it has comparable hardness. Its hardness is nearly 30 times smaller with a Vickers hardness approximately 350 $Kgmm^{-2}$ compared with about 10000 $Kgmm^{-2}$ for diamond [48]. Even so it is unlikely that material with bulk modulus smaller than that of diamond will be harder.

The shear modulus describes the resistance of a material to anisotropic shape change and plays an important role in the elastic theory of dislocations. It is more pertinent to hardness, but it is more complex property. It is more complex, because it depends on both the plane of shear and the direction of shear. It indicates how well a material resists a tearing force [49]. It was confirmed experimentally as being the best hardness

predictor, as already mentioned in chapter two. Aluminum, for example, has fairly large bulk modulus but is not considered a hard material because its shear modulus small. Pugh [50] introduced the ratio between the shear and bulk modulus, *G/B*, for polycrystalline phases, as a measure of toughness /fracture in metals. A low (high) *G/B* value is also often associated with ductility (brittleness).

In mineralogy, hardness is measured on the Moh scale, which is based on the scratch tests with the use of certain standard substances from talc to diamond. This scale is nonlinear and in this hardness is not reliable because materials of similar hardness can scratch each other and the resulting value depends on the specific details of the contact between the two materials. A more accurate way of defining and measuring hardness is by the indentation of the material by a hard indenter; in this different methods are used: the Brinell, the Rockwell, the Vickers and the Knoop. Usually the Brinell hardness testing is used to determine the hardness metal forgings and castings that have large grain structures. The Rockwell hardness testing is more commonly used in industry because the hardness is read directly off the machine. The Vickers and the Knoop hardness testing are widely used for determining the hardness of materials that are too small. The difference between Vickers and the Knoop tests is the shape of the diamond pyramid indenter. The Vickers and the Knoops indenter methods are the frequently used. Materials with hardness of above 40 GPa are known to be superhard. The hardness of diamond is 90 GPa, and the second hardest material c-BN, with hardness of

50 GPa [14]. Hard materials have many industrial applications wherever resistance to abrasion and wear are important, and are then intensively investigated both experimentally and theoretically. Combining high hardness with other properties, such as chemical inertness and low-cost synthesis, could quickly yield practical benefits, for example, by providing a replacement for cubic boron nitride for cutting and polishing steel.

4 Theoretical methods

4.1 Introduction

Computer simulation techniques are used in areas of condensed matter physics, materials science, chemical physics, physical chemistry, biological science and engineering science. These techniques enable simulator to develop and explore models of structures, energetic and dynamic of complex molecules and materials, with high accuracy. Simulation techniques are increasingly integrated with the experimental synthetic and characterization studies. The capability and power of modern computer technology, allows one to attain more and more information about the model. Even systems which were not treatable some years ago can be considered now. This made it possible to perform calculations for real material with accuracy and thus they can provide meaningful detailed comparison to the experimental measurements

The computer modeling at atomic and molecular level can be divided into two methods, namely: the forcefields methods and electronics structure methods (quantum mechanical methods). For predicting the properties of materials the atomistic technique

is significant. Firstly for simulation and prediction of structural and functional properties, the choice is between the forcefields and quantum mechanical methods. Although, force field methods are preferably because of the high computational efficiency, they have not been successfully developed for metal oxynitrides, so the quantum mechanical based methods is employed in this research. The quantum mechanical methods is divided into semi-empirical and ab-initio methods. However, in this work, as already mentioned in chapter one we rely on ab-initio methods, particularly the DFT.

4.2 Density functional theory (DFT)

Density functional theory (DFT) methods are the most widely used ab-initio methods in computational material science and solid state physics because of their computational efficiency and very good accuracy. DFT is powerful in determining the electronic structural properties of atoms, molecules, and solids in their ground state using the Kohn, Hohenberg, and Sham [51, 52]. In DFT, the total energy is expressed in terms of the total electron density rather than the wave function. The total energy is decomposed into three contributions, a kinetic energy, a coulomb energy due to electrostatic interaction among all charged particles in the system, and a term called the exchange-correlation energy. This decomposition is formally exact, but the actual expressions for the many body exchange and correlation interactions are unknown. In DFT, the total

electron density is decomposed into one electron densities, which are constructed from one electron wave functions. These one electron wave functions are similar to those of Hartee-Fock theory.

Hohenberg and Kohn (1964) working together investigated the foundation of Thomas-Fermi model, [53] where they formulated and gave proofs of two important theorems.

The Hohenberg-Kohn first theorem state: the external potential $V_{ext}(r)$ is determined, within a trivial additive constant, by the electron density $\rho(r)$.

The proof of this theorem is as follows:

Let consider an external potential $V_{ext}(r)$ with the ground state wave function ψ that gives an electron density $\rho(r)$. Suppose there is another external potential $V_{ext}^{'}(r)$ with the ground state wave function $\psi^{'}$ gives the same density $\rho(r)$. We are here supposing that the states are non-degenerate. The external potential would give two different Hamiltonians $\hat{H}$ and $\hat{H}^{'}$ whose ground state density would have different wave functions ψ and $\psi^{'}$. Consider

$$E_o = \langle \psi | \hat{H} | \psi \rangle < \langle \psi^{'} | \hat{H} | \psi^{'} \rangle = E_o^{'} \qquad 4.1$$

Where

$$\left\langle \psi' \left| \hat{H} \right| \psi' \right\rangle = \left\langle \psi' \left| \hat{H} - \hat{H}' \right| \psi' \right\rangle + \left\langle \psi' \left| \hat{H}' \right| \psi' \right\rangle$$

$$= \int \rho(r)\left[V_{ext}(r) - V'_{ext}(r)\right]dr + E'_o \qquad 4.2$$

The latter follows from the definition of H and H' the definition of ρ.

On the other hand if we consider E'_o in exactly the same way, we find the same kind of equation, with $V_{ext}(r)$ and $V'_{ext}(r)$ interchanged,

$$E'_o = -\int \rho(r)\left[V_{ext}(r) - V'_{ext}(r)\right]dr + E_o \qquad 4.3$$

Addition of 4.2 and 4.3 leads to the results $E_o + E'_o < E'_o + E_o$ which are a contradiction and so there cannot be two different $V_{ext}(r)$ that give the same $\rho(r)$ for their ground state. This means that the density is a unique functional of the potential. So $\rho(r)$ determines *N* and $V_{ext}(r)$ and hence all properties of the ground state.

Second Theorem State: The ground state energy can be obtained variationally. The density that minimizes the total energy is the exact ground state density.

Consider the total ground state energy of a system that can be written as

$$E\left[\rho(r)\right] = V_{ext}\left[\rho\right] + T\left[\rho\right] + U_{ee}\left[\rho\right] \qquad 4.4$$

Where $V_{ext}[\rho]$ is the external potential energy, $T[\rho]$ is the kinetic energy, and $U_{ee}[\rho]$ is the electron-electron interactions.

Defining:-

$$V_{ext}[\rho] = \int V_{ext}(r)\rho(r)dr \quad , \qquad 4.5$$

And the quantity

$$F[\rho(r)] = \langle \psi | \hat{F} | \psi \rangle, \qquad 4.6$$

The functional $F[\rho]$ is the universal in the sense that it does not depend on the external potential and the operator $\hat{F}$ stand for the kinetic energy and the electron-electron interactions. ψ is a functional of $\rho(r)$, a density that is the ground-state that corresponds to some $V_{ext}(r)$ is known as *V*-representable. Thus,

$$E_{V(r)}[\rho(r)] = \int \rho'(r)V(r)dr + F[\rho'(r)] \qquad 4.7$$

And by variation principle,

$$\langle \psi' | \hat{F} | \psi' \rangle + \langle \psi' | \hat{V}_{ext} | \psi' \rangle > \langle \psi | \hat{F} | \psi \rangle + \langle \psi | V_{ext} | \psi \rangle \qquad 4.8$$

Where the ground state energy (ψ), stand for the wavefunction associated with the correct ground state density $\rho(r)$. This leads to,

$$\int V_{ext}(r)\rho'(r)dr + F[\rho''(r)] > \int V_{ext}(r)\rho(r)dr + F[\rho(r)], \qquad 4.9$$

This is the Hohenberg-Kohn energy variational principle,

$$E_V[\rho'(r)] \geq E_V[\rho(r)] \qquad 4.10$$

Although the Hohenberg-Kohn theorem shows it is possible to use the ground state density to calculate properties of the system, they do not offer a way of computing the ground state density. In the following year Kohn-Sham [52] came with the solution.

4.2.1 Kohn –Sham Equations

The work of Kohn-Sham [52] allows us to calculate the true density of the system by solving a set of self consistent one body equations. Kohn-Sham separated $F[\rho(r)]$ into three distinct parts, so the total energy functional can be written as:

$$E[\rho(r)] = T[\rho(r)] + \frac{1}{2}\iint \frac{\rho(r)\rho(r')}{|r-r'|} dr dr' + E_{XC}[\rho(r)] + \int \rho(r) V_{ext}(r) dr \qquad 4.11$$

Where, $T[\rho(r)]$ is the kinetic of a system of non-interacting electron gas with density $\rho(r)$, $\frac{1}{2}\iint \frac{\rho(r)\rho(r')}{|r-r'|} dr dr'$ is the classical electrostatic (Hatree) energy of electrons and $E_{XC}[\rho(r)]$ is the energy of exchange and correlation, which contains the difference between the exact and non-interacting kinetic energies and also the non-classical contribution to the electron-electron interactions, of which the exchange is a part.

$$T[\rho(r)] = \frac{1}{2}\sum_{m=1}^{N}\int \psi_m^*(r)\nabla^2\psi_m(r)dr \quad , \qquad 4.12$$

This is not the kinetic energy of the real system. Introducing a normalization constraint on the electron density, $\int \rho(r)dr = N$, we get

$$\frac{\delta}{\delta\rho(r)}\left[E[\rho(r)] - \mu\int \rho(r)dr\right] = 0 \qquad 4.13$$

$$\Rightarrow \quad \frac{\delta E[\rho(r)]}{\delta\rho(r)} = \mu \qquad 4.14$$

Where μ is the Lagrange parameter associated with the restriction of the density to yield the correct total number of electrons *N*. In terms of an effective potential, $V_{eff}(r)$, equation 4.14 becomes

$$\mu = \frac{\delta T\rho(r)}{\delta\rho(r)} + V_{eff}(r) \qquad 4.15$$

Where the effective potential $V_{eff}(r)$ is given by,

$$V_{eff}(r) = V_{ext}(r) + \int \frac{\rho(r')}{|r - r'|}dr' + V_{XC}(r) \qquad 4.16$$

This effecting one electron potential has contributions from the ion-electron interaction, while the electron-electron interaction is divided into the Hartree term and the exchange and correlation potential $V_{XC}(r)$.

and

$$V_{XC}(r) = \frac{\delta E_{XC}[\rho(r)]}{\delta \rho(r)} \qquad 4.17$$

The problem of finding the ground state of an interacting many particle systems is therefore mapped into a mean field problem where non-interacting electrons are moving in an effective potential set up by all valence electrons in the material. The resulting Kohn-Sham orbital Schrödinger equations:

$$\left[-\frac{\hbar^2}{2m}\nabla^2 + V_{eff}(r) - \in_m \right] \psi_m = 0 \qquad 4.18$$

are solved self-consistently and the ground state electron density is determined by the one electron wave functions,

$$\rho(r) = \sum_{i=1}^{N} |\psi_m(r)|^2 , \qquad 4.19$$

The self-consistent scheme is an iterative process to obtain the correct electron density which minimizes the total energy of the system. Self-consistent solution is required since $\rho(r)$ is used to calculate $V_{eff}(r)$ by equation 4.16 and $V_{eff}(r)$ is then inserted in the Kohn-Sham equations.

The above equations provide a theoretical exact method for finding the ground state energy of an interacting system provided the form of E_{XC} is known. Generally the form of E_{XC} is unknown and its exact value has been evaluated for very few simple systems.

Usually E_{XC} in the electronic structure calculations is approximated within local density approximation or generalized-gradient approximation. Now we turn to the next section.

4.2.2 The Local Density approximation

The simplest and easiest approximation method for the exchange and correlation energy function is the local-density approximation (LDA), proposed by Kohn and Sham [52]. Using the LDA the exchange and correlation energy for density a density $\rho(r)$ is given by:

$$E_{xc}^{LDA}[\rho] = \int \rho(r)\varepsilon_{xc}(\rho(r))dr \qquad 4.20$$

Where $\varepsilon_{xc}(\rho(r))$ indicates the exchange and correlation energy per particle of a uniform electron gas of density $\rho(r)$. The corresponding exchange and correlation potential is then given by:

$$V_{xc}^{LDA}[\rho(r)] = \frac{\delta E_{xc}^{LDA}}{\delta \rho(r)} = \varepsilon_{xc}(\rho) + \frac{\rho(r)\partial \varepsilon_{xc}(\rho)}{\partial \rho} \qquad 4.21$$

The quantity $\varepsilon_{xc}(\rho(r))$ can further be divided into exchange and correlation contributions,

$$E_{xc}(\rho(r)) = \varepsilon_x(\rho(r)) + \varepsilon_c(\rho(r)). \qquad 4.22$$

The exchange part ε_x was derived by Bloch and Dirac [54, 55] to be

$$\varepsilon_x = \frac{-3}{4}\left[\frac{3\rho(r)}{\pi}\right]^{1/3} \quad 4.23$$

$$= Cx\,\rho(r)^{1/3} \quad 4.24$$

Where C is

$$C = \frac{-3}{4}\left[\frac{3}{\pi}\right]^{1/3} \quad 4.25$$

Accurate values of $\varepsilon_c(\rho)$ were calculated by Ceperly and Alder using Quantum Monte Carlo technique [56]. The exchange and correlation energy functional is assumed to be purely local in the LDA. LDA is exact in the limit of high density or varying density distribution and works quite well also for the description of weakly correlated materials. In strongly correlated systems the LDA approach is not sufficient any more and strong interelectronic correlation may be included by adding an empirical energy U to the LDA scheme (LDA +U method). Alternatively a possible improvement upon LDA is the inclusion of the dependence of the gradient of the density, the so called generalized gradient approximation, which will be discussed in the next section.

4.2.3 The Generalized Gradient Approximation (GGA)

In fact the generalized gradient approximation (GGA) is the only gradient correction of the LDA method. Symbolically this can be written as:

$$E_{xc}^{GGA}[\rho,\rho] = \int f(\rho_\alpha, \rho_\beta, \nabla\rho_\alpha, \nabla\rho_\beta)dr. \qquad 4.26$$

Like LDA, it is common to split GGA into exchange and correlation contributions

$$E_{xc}^{GGA} = E_{x}^{GGA} + E_{c}^{GGA} \qquad 4.27$$

In GGA only the exchange and correlation energy $E_{xc} = E_x + E_c$ as a functional of electron spin densities ρ_α, ρ_β must be approximated [57]. Where ρ_α and ρ_β are respectively, the density of spin up and spin down. For structural properties of real material the GGA have been widely used and have proved to be quite successful in correcting some defect of the LDA. GGA do not offer a consistent improvement over LDA in all types of system, but they have been shown to improve on the LDA for calculation of the total energy and bond length of many systems.

In this work we have employed the widely used GGA in the market, the so called PBE due to Perdew, Burke and Ernzerhof [57, 58]. First, the enhancement factor F_{XC} over the local exchange is defined:

$$E_{XC}^{PBE}[\rho] = \int \rho(r)\varepsilon_X^{LDA}[\rho(r)]F_{XC}(\rho,\zeta,s)dr \qquad 4.28$$

Where ρ is the local density, ζ is the relative spin polarization and $s = |\nabla\rho(r)|/(2k_F\rho)$ is the dimensionless density gradient, as in Perdew-Wang 1986, PW86 [59]:

$$F_X(s) = 1 + k - \frac{k}{1 + \mu s^2 / k} \qquad 4.29$$

Where $\mu = \beta(\pi^2/3) = 0.21951$ and $\beta = 0.066725$ is related to the second order gradient expansion [60]. This form is chosen since it

- Satisfies the uniform scaling condition,
- Recovers the correct uniform electron gas limit because $F_X(0) = 1$,
- Obeys the spin-scaling relationships,
- Recovers the local spin density approximation (LSDA) linear limit for $s \to 0 (F_X(s) \to 1 + \mu s^2)$, and
- Satisfies the local Lieb-Oxford bound [61], $\varepsilon_X(r) \geq -1.679\rho(r)^{4/3}$, that is, $F_X(s) \leq 1.804$, for all r, provided that $k \leq 0.804$. PBE chooses the largest allowed value, $k = 0.804$.

On the otherhand the correlation energy is written in the form similar to PW91 [60], that is,

$$E_c^{PBE}[\rho] = \int \rho(r)\left[\varepsilon_C^{LDA}(\rho,\zeta) + H[\rho,\zeta,t]\right]dr \qquad 4.30$$

With

$$H[\rho,\zeta,t]=\left(\frac{e^2}{a_0}\right)\gamma\phi^3 In\left\{1+\frac{\beta\gamma^2}{t}\left[\frac{1+At^2}{1+At^2+A^2t^4}\right]\right\} \qquad 4.31$$

Here, $t=|\nabla\rho(r)|/(2\phi k_s\rho)$ is a dimensionless density gradient, $k_s=(4k_F/\pi)^{1/2}$ is the TF screening wave number and $\phi(\zeta)=\left[(1+\zeta)^{2/3}+(1-\zeta)^{2/3}\right]/2$ is a spin-scaling factor. The quantity β is the same as for the exchange term β=0.066725, and $\gamma=(1-In2)/\pi^2=0.031091$. The function *A* has the following form:

$$A=\frac{\beta}{\gamma}\left[e^{-\varepsilon_C^{LDA}[\rho]/(\gamma\phi^3e^2/a_0)}-1\right]^{-1} \qquad 4.32$$

So defined, the correlation correction term H satisfies the following properties:

- It tends to the correct second-order gradient expansion in the slowly varying (high-density) limit $(t\to 0)$,
- It approaches minus the uniform electron gas correlation $-\varepsilon_C^{LDA}$ for rapidly varying densities $(t\to\infty)$, thus making the correlation energy to vanish (this results from the correlation hole sum rule),
- It cancels the logarithmic singularity of ε_C^{LDA} in the high-density limit, thus forcing the correlation energy to scale to a constant under uniform scaling of the density.

4.2.4 General comparison of LDA and GGA

The behavior of the LDA relative to the GGA is well understood on the basis of the many comparative studies that have been done. The LDA is generally very successful in predicting structures and macroscopic properties, but some shortcomings are notorious as well [62]. These concern in particular:

- Energies of exited states and in particular band gaps in semiconductors and insulators are systematically underestimated. This after all not so surprising since DFT is based on theorem referring to the ground state only.
- There is a general tendency to overbinding, i.e. cohesive energies are significantly overestimated and lattice parameters are underestimated by up to 3%.
- The wrong ground state is predicted for some magnetic systems (the most notable example is Fe which is predicted to be hexagonal close packed and non-magnetic instead of body-centered cubic and ferromagnetic) and for strongly correlated system (e.g. the Mott insulators NiO and La_2CuO_4 are predicted to be metallic in the LDA).
- Van der Waals interactions are not approximately described in the LDA, although there are some recent suggestions for overcoming this problem [63-65].

Generally the GGA try to improve the LDA, from the results of many studies, the following conclusion may be drawn [7]:

- GGAs significantly improve the ground state properties of light atoms and molecules, clusters and solid composed of them.
- Many properties of *3d* transition metals are greatly improved; for example, unlike the local spin density approximation (LSDA) the correct *bcc* ground state of Fe is obtained.
- The description of Mott-Hubbard insulators, like the undoped phases of high-T_c cuprates, is not significantly improved over the LSDA.
- GGA functional usually favor magnetism more than the LSDA, and as result the magnetic energies for some *3d* transition metals may be overestimated.
- Lastly the structural properties are generally improved, although GGAs sometimes leads to overcorrection of the LDA errors in the lattice parameters.

4.3 Pseudopotentials

Working with transition metal involves dealing with large number of electrons, so the computational time increases exponentially as the system size increases. “Fortunately” the chemical bond does not strongly depend on the core electrons. In fact, only the bonding energy is affected by the average electrostatic potential generated in the vicinity of the core. The aim is then to model the core electrons and their interaction with the other electrons. The concept of pseudopotentials was introduced by Fermi [66]

to study high lying atomic states. In the following year, Hellman [67] proposed that pseudopotentials be used for calculating the energy levels of the alkali metals. But the wide spread usage of pseudopotentials did not occur until the late 1950s, where Phillips and Kleinman introduced pseudopotential approach [68] with the orthogonalized plane waves (OPW) method [69]. In the OPW method the valence wavefunctions were expanded using a basis consisting of plane waves that were orthogonalized to the lower lying core state. This concept of pseudopotential was extended and led to the development of pseudopotential methods such as norm-conserving pseudopotentials, ultrasoft pseudopotentials (US-PP) and the projector augmented wave (PAW) method, which will be discussed below (in this chapter).

Generally the electrons in the outermost shell (the valence electrons) are the one in which actively participating in determining the chemical and physical properties of molecules and solids. This has led to the idea behind the pseudopotential theory to simulate the interaction between valence electrons and ion cores, considering the latter as frozen. Thus the ion-ion interaction can be considered as purely electrostatic. The main goal of pseudopotential is to simplify electronic structure calculations by eliminating the need to include atomic core states and the strong potentials responsible for binding them. Pseudopotentials allow one to ignore the core electrons, at the expense of the replacement of the strong nuclear coulomb potential of the all electron system by a weak pseudopotential, designed to mimic the scattering due to the

combined effect to nuclei and core electrons [70]. A further advantage of pseudopotentials is relativistic effects can be incorporated easily into the potential while further treating the valence electrons non-relativistic. A pseudopotential that uses the same potential in each angular momentum channel is called a local pseudopotential. Local pseudopotentials are computationally much more efficient than nonlocal one. One of the important concepts in pseudopotential applications is the degree of hardness of pseudopotential. Pseudopotential is considered soft when it requires a small number of Fourier components for its accurate representation and hard otherwise.

Pseudopotentials are intertwined with plane wave methods because they allow calculations to be done with a feasible number of plane waves. The basic ideas can be understood in terms of empirical pseudopotentials which provide a compact description of bands in terms of a few Fourier components of the potentials. The simplicity of the plane waves leads to very efficient numerical schemes for solving the Kohn-Sham equations, and the employment of pseudopotentials guarantees that the wave functions can be expended in a relatively small set of plane waves. Plane waves are the exact eigenfunctions of the homogeneous electron gas. Therefore, plane waves are the natural choice for simple metals where the ionic cores can be viewed as rather small perturbations to the homogeneous electron gas. Plane waves are orthonormal and energy independent. Hence, upon a basis set expansion the Schrödinger equation transform into a simple matrix eigenvalue problem for the expansion coefficients. A

further advantage of plane waves is that they are unbiased to any particular atom. Since plane waves do not depend on the position of the atoms, the Hellmann-Feynman [71] theorem can be applied directly to calculate atomic forces; even for a non-complete basis set the Pulay [72] terms are identical zero. The main disadvantage of a pure plane wave approach is that the correct descriptions of the strong oscillations of the wave functions close to the nucleus require a superposition of plenty of plane waves. This, however is a very resource-consuming procedure and not suitable for common quantum chemistry calculations. In order to simplify the strong oscillations of the wave function close to the nucleus, they are substituted by a much smoother pseudo wave function. This is accomplished by a substitution of the true potential inside the corer by a suitable pseudopotential. The convergence of the calculation can be improved by extending the cut-off energy (i.e. the highest kinetic energy of the plane waves. For planes waves approaches to be of practical use the coulomb potential of the electron nucleus interaction should be replaced by pseudopotential. Plane waves are often the basis of choice for development of new methods, such as Car-Parrinelo [73] quantum molecular dynamics simulations, efficient iterative methods and many other innovations because of its simplicity. The fact that pseudopotential are not unique allows the freedom to choose forms that simplify the calculation and the interpretation of the resulting electronic structure. The advent of “ab-initio norm conserving” and “ultrasoft” pseudopotentials has led to accurate calculations which form basis for much current research and development of new methods in electronic structure calculation [74].

4.3.1 Norm conserving pseudopotentials

The norm conserving pseudopotential methods has attracted much attention recently due to its simplicity, elegance and computational efficiency. The simplicity and efficacy of pseudopotentials have evolved considerably since the Phillips and Kleinman [68] construction. This evolution has been driven, by the following goals. Firstly all the pseudopotential should be soft as possible, meaning that it should allow expansion of the valence pseudo-wavefunctions using as few planewaves as possible; secondly it should be as transferable as possible (meaning that a pseudopotential generated for a given atomic configuration should reproduce others accurately), thereby helping to assure that the results will be reliable in solid state applications, where the crystals potential is necessarily different from an atomic potential; and the pseudo-charge density (the charge density constructed using pseudo-wavefunctions) should reproduce the valence charge density as accurately as possible. The pseudo-wavefunctions (and potential) are constructed to be equal to the actual valence wavefunctions (and potential) outside some core radius, with norm conserving pseudopotentials. The pseudo-wavefunctions differ from the true wavefunctions, inside the core radius, but the norm constrained to be the same [7]. Norm conserving pseudopotentials are normalized and are the solution of Schrödinger equation with a model potential chosen

to reproduce the valence properties of the atom given by all-electron calculation. The norm conserving pseudopotentials displays several fundamentals properties. They are calculated from ab-initio self-consistent atomic potential based on local density functional (LDA) theory. They produce pseudo-wavefuctions which are identical to real wave functions beyond r_c, a chosen core radius, whose eigenvalue agree with the real energy eigenvalue. Additionally the integrals from 0 to r of the real and pseudo charge densities agree for $r > r_c$ for each valence state (norm conservation). The logarithmic derivatives of real derivatives of the real and pseudo-wavefunction and their first energy derivatives agree for $r > r_c$. Last two properties are crucial for the generation of good transferable potential [75]. The requirement of the norm conservation is key step in making accurate, transferable pseudopotentials, which is essential so that a pseudopotential constructed in one environment can faithfully describe the valence properties in different environments including atoms, ions and molecules.

4.3.2 Ultrasoft Pseudopotentials

The idea of ultrasoft pseudopotentials as put forward by Vanderbilt [76] is that the relation of the norm conservation can be used to generate much softer potentials, i.e. the basis set size can be made substantially smaller. In this scheme the pseudo-

wavefunctions can be made softer within the core region, so that the cutoff energy can be reduced dramatically. The pseudopotential transferability is maintained by introducing a generalized orthonormality condition. The augmentation chargers are normally "pseudized" to make calculations feasible. It has been rigorously proven [77] that without such pseudization, i.e. in the limit of very accurate augmented chargers, the ultrasoft pseudopotential method should and in fact does reproduce the results of the all electron projector augmented wave (PAW) method [6]. Ultrasoft potentials have another advantage in addition to being much softer than the norm conserving potentials. The generations algorithm for ultrasoft produces Kleinman-Bylander [78] separable for more than one projector function in each angular momentum channel, which guarantees good scattering properties over a prespecified energy range. This results in much better transferability and accuracy of pseudopotentials. Ultrasoft potentials usually treat "shallow" core electrons as valence states by including multiple set of occupied states in each angular momentum channel. Nonlinear core corrections can used to describe shallow core state in a more approximate way if computational cost becomes an issue [79]. The ultrasoft pseudopotential formulation is more complex than the formalism for norm conserving pseudopotentials. In particular, one has to solve a generalized eigenvalue problem as a result of using nonorthogonal wave functions. On the other hand, ultrasoft potentials provide great improvements in both accuracy and computational cost for elements with the valence *1s, 2p, 3d* or *4f* electrons where the norm conserving potentials are necessarily quite hard [80].

4.3.3 Projector Augmented Waves (PAW)

The projector augmented wave (PAW) method was developed by Bloch [6], as a very powerful tool for performing electronic structure calculations of density functional theory. The PAW method is an extension of augmented wave methods and the pseudopotential approach, which combine their traditions into a unified electronic structure method. Like the ultrasoft pseudopotential method, it introduces projectors and auxiliary localized functions. The PAW approach also defines a functional for the total energy that involves auxiliary functions and it uses advances in algorithms for efficient solution of the generalized eigenvalue problem. However, the differences is that the PAW approach keeps the full all-electron wavefunction in a form similar to the general OPW expression, since the full wave function varies rapidly near the nucleus, all integrals are evaluated as a combination of integrals of smooth functions extending throughout space plus localized contributions evaluated by radial integration over muffin-tin spheres. It maintains the advantage of pseudopotentials that forces can be calculated easily. It combines some of the best features of pseudopotentials and all-electron approaches. The Ultrasoft pseudopotentials and the PAW methods permit accurate calculations with a smaller set of planewaves. Unlike pseudopotentials, the PAW method keeps the entire set of all-electrons core functions and smooth parts of the

valence function. The problem of constructing the projector and basis functions needed for PAW approach is very similar to the problem of constructing local and nonlocal pseudopotentials.

The comparison of the PAW approach with the norm conserving pseudopotential calculations and local basis set calculations indicates the following [81]:

- The accuracy of the PAW is similar to the accuracy of local basis calculation.
- The convergence with respect to the plane wave basis set leads to practical calculations even for difficult systems (transition metal).
- The bonding properties in transition metals are described correctly for wide range of bond distances, from diatomic molecules to solids.
- The accuracy of the calculations can be systematically improved by expanding the local representation.
- The method is robust with respect to the choice of local basis set.
- Local basis set terms in the Hamiltonian are one centered and can be precomputed so that execution times are similar to the plane wave pseudopotential methods.

The accuracy of the methods depends on two factors: the completeness of plane wave basis with respect to the smooth wave function and the completeness of basis set in the atomic sphere region. The size of the plane wave basis is typically characterized by the energy cutoff, the kinetic energy of the highest in the basis set. As the energy cutoff

increases, the errors due to incompleteness of the plane wave basis become smaller. In the PAW method the plane wave basis errors are determined the smoothness of basis set, since in order for various cancellations to occur the plane wave basis representation of basis set depends on the size of the atomic sphere as well as the strength of the effective atomic potential. The convergence of the pseudopotentials methods can be greatly improved by removing the norm conserving condition via Vanderbilt's ultrasoft pseudopotentials [76] or Blochl's PAW method [6]. As discussed by Blochl and later by Kresse and Joubert [77], there are certain similarities between ultrasoft pseudopotentials and PAW method. From a numerical point of view both methods should have roughly the same efficiency. However, there are several advantages associated with all electron nature of PAW approach. Firstly, the issue of parameterizing the pseudopotential is avoided in PAW, of which this can be difficult in Vanderbilt's method [76]. Secondly, the accuracy of the PAW approach can be systematically improved by increasing the size of the local basis set. Thirdly, the PAW approach provides all-electron Kohn-Sham wave functions that are necessary in certain applications.

4.4 Vienna Ab-initio Simulation Package CODE

VASP (Vienna Ab-initio Simulation Package) is a package for performing ab-initio quantum-mechanical molecular dynamics (MD) simulations using Pseudopotentials or

PAW and plane waves basis set. VASP is leading the ab-initio method for predicting crystal and molecular structures, relative phase stabilities and electronic and magnetic properties. In VASP, the Kohn-Sham equations are solved self consistently with an iterative matrix diagonalisation and the Pulay/Broyden [82, 83] mixing method for charge density. Combining these two techniques makes the code very efficient especially for transition metal systems that present a complex band structure around the Fermi level. The algorithms implemented in VASP are based on the conjugate gradient scheme, the block Davidson scheme or a residual minimization scheme (RMM). These algorithms calculate the electronic ground state for a given geometry, calculate forces, and based on these forces, and predict a new geometry. These steps are then repeated until an energy criterion is ignored and only the forces are minimized.

The interaction between ions and electrons is described by ultra-soft Vanderbilt pseudopotential (US-PP) or by the projector-augmented wave (PAW) method [76, 6]. US-PP (and the PAW methods) allow for a considerable reduction of the number of plane-waves per atom for transition metals and first row elements. The Hamiltonian is determined in pieces in direct and reciprocal space. Fast Fourier Transformations (FFT) is used to switch from direct to reciprocal space and vice-versa. This allows for partial diagonalisation. Besides the pure local density (LDA, several gradient-corrected functional are implemented in VASP to account for the non-local in the exchange correlation (BP, PW91, PBE).

The number of K-points in the irreducible part of the Brillouin zone has a great influence on the accuracy of the calculations. This makes it clear that the sampling set should be chosen very carefully. The K-points sample is usually calculated by the program using the Monkhorst-Pack method [84]. To improve the convergence with respect to the K-points sampling several techniques can be used: the linear tetrahedron method, smearing methods such as finite temperature approaches or improved functional form (Methfessel and Paxton method [85], and finite methods such as Gaussian of Fermi smearing).

5 Transition Metal Oxynitrides

5.1 Transition metal oxynitrides

Within recent years, transition metal oxynitrides have attracted increased interest because of their physical and chemical properties, offering a great potential for industrial application [87-89]. Oxynitrides are an under-explored class of mixed anion solids which show novel structures and may have unusual physical properties [90]. For example, the replacement of O by N may adjust the colour of some 4d and 5d transition metal oxynitrides and these oxynitride materials have potential as safe pigment materials to replace currently used toxic metal containing pigment materials [91-93]. They are promising candidates for future application as ion conductor materials (sensors) and colour pigments [94]. In addition Oxynitrides of early transition metals are bifunctional catalysts active in hydrodenitrogenation (HDN) [95, 86]. Catalytic HDN is a process of nitrogen removal from hydrocarbon feedstock. Oxynitrides are simply obtained from metal oxide and ammonia [86] and they are able to have the same structure type of the parent. Combining the beneficial properties of nitrides (hardness) and oxide (chemical stability) gives the possibility to tune the properties of the resulting oxynitride by changing the oxygen/nitrogen content in transition metal oxynitrides.

Transition metal oxynitrides and oxycarbides are usually found as intermediates, in some cases as final product, during the synthesis of the corresponding metal nitrides and carbides [96]. Aguiar *et al* [97] dealt with perovskites oxynitrides of the ABO_2N type (A = C^{2+}, Sr^{2+}, Ba^{2+} and B = Ta^{5+}, Nb^{5+}), these materials show a large range of colour and are stable in air, water or diluted acids at room temperature. They also have advantage of not containing toxic metals and, in turn, are eco-friendly. Peroskites oxynitrides are stable at very high temperature [97]. From the oxide to oxynitrides, the anionic substitution of divalent oxygen for trivalent nitrogen causes an increase in the covalency of M-O/N bonds giving rise to marked modification on the structural, transport, optical and magnetic properties of the resulting oxynitrides [98].

5.2 Metal oxides

The high pressure phases of metal oxides typically exhibit very high bulk moduli and are candidates for hard materials. Of the various metal oxide that have now been considered, ZrO_2 and HfO_2 are reported to have potential superhard high-pressure phase, and therefore are hold potential as refractory materials [99]. Looking to the entire metal oxides, zirconia is the most studied now having extensive range of industrial application [23, 100, and 101]. Zirconia has a monoclinic ambient phase with several important phase formed under extreme conditions [4]. The studies of Lerch *et al* [102, 103] are notably valued in the case of zirconium oxynitrides. They show

oxynitrides with a high ionic conductivity, comparable with yttria stabilized cubic ZrO_2, could be obtained by a high temperature reaction of ZrO_2, with nitrogen [102, 103]. Metal oxides have been examined for their potential hard properties and TiO_2 in the cotunnite structure has been identified as the hardest known oxide synthesized to date [26]. It has found to have bulk modulus and hardness of 431 GPa and 38 GPa respectively. TiO_2 has been suggested as a material that could have a series of high-pressure phases with a hardness possibly approaching that of diamond [104, 105].

There are strong differences found for the metal dioxide and similar oxynitrides depending on the metal's character. In the case of metal dioxides (MO_2) it is likely that as the metal coordination increases so does the bulk modulus. The highest coordination in the metal dioxides is the cotunnite structure in which the metal atom is coordinated by nine oxygen's [106]. Actually it may be that the cotunnite phase of the metal atom is the highest coordination phase that can be achieved in MO_2 series and therefore could represent the hardest possible structure. Given the greater potential of highly coordinated MO_2 cotunnite phase as an ultrahard material, the possibility of changing the chemical nature of this phase through incorporation of other elements may lead to another potentially important series of ultrahard materials.

In relation to nitrides, generally bonding among solid nitrides is less ionic than in the corresponding oxide. Main group nitrides compounds are often wide-gap

semiconductors where as oxides are usually insulators. Transition metal oxide tend to be highly refractory due to their ionic bonding, but generally they are less refractory than their corresponding nitrides and also have low hardness (for example TiO_2 and ZrO_2 versus TiN and ZrN) [107].

5.3 Metal nitrides

Transition metal nitrides have many outstanding physical properties of refractory ceramics in the past, such as high melting, high hardness, and tensile strength. Most transition metals form nitride at high temperatures and at either ambient or high pressure (for example, ZrN, Vn, MoN) [30]. When transition nitrides belong to group IVb or Vb in the periodic table, binary transition metal nitrides form rock salt structure. At nanoscale level, they display three types of bonding characteristics; metallic, ionic and covalent. The fact that nitrogen is less electronegative than oxygen leads to more covalent bonding in nitrides and oxynitrides than in oxides. Substitution of nitrogen for oxygen modifies the band structure and if the highest oxidation state of transition metal can be stabilized, for example tantalum in $SrTa_3ON$, often results in the colour of the nitride type compound being different from that of corresponding oxide [108]. The structure of the spinel nitrides are of significant interest and are most likely to be formed at high temperature and high pressure [109]. Double nitrides AB_2N_4 are most likely stable when the counterparts BA_2N_4 are metastable. All of the stable double

nitrides show higher covalency than their constituent single nitrides. Some of the compounds show a bulk modulus exceeding 300 GPa, for example c-TiC_2N_4 (317 GPa), c-SiC_2N_4 (327 GPa) and etc [109].

High thermal stability is one of many important properties required for industrial applications of hard and superhard coating on cutting tools [24, 110]. Silicon nitride (Si_3N_4) has attracted much attention because of its advanced mechanical, electronic and thermal properties. It was reported that cubic spinel (γ-SiN_4) with cubic spinel structure could be synthesized at pressure above 15 GPa and temperature exceeding 2000 K, yet persists metastably in air at an ambient pressure to at least 700 K. the hardness of the nitride spinel has been predicted by the chemical bond definition of spinel [10].

6 Calculational Results on Oxynitrides of Tantalum, Niobium, Tungsten and Titanium

As discussed earlier a combination of the metal oxide and metal nitride could produce phases with properties better than the parent oxide or nitride. In this section we apply DFT within LDA and GGA to look at several metal oxynitrides. The goal is to examine properties of the oxynitride phase and to estimate the pressure needed for a synthesis of such phase. In particular we estimate the compressibility of each phase. In our calculation the functional relationship for pressure against volume is called the equation of state (EOS). Usually the EOS of solids describes the relationships among thermodynamically variables such as pressure, temperature, and volume. It provides numerous information of non-linear compression of material at high pressure. The high pressure EOS has been represented in various functional, such as, the Murnaghan [111], Birch-Murnaghan [112], and Vinet Universal equation [113]. They all give very similar results.

In our calculation we used Birch-Murnaghan [112] EOS. This approach expands the Gibb's free energy in terms of Eulerian strain ϵ, with $V_o \big/ V = (1-2)^{3/2}$. The integrated energy volume form of the third order Birch-Murnaghan [104] EOS becomes

$$E(V) = \frac{-9}{16} B_o \left[\left(4 - B_o^{'}\right) \frac{V_o^3}{V^2} - \left(14 - 3B_o^{'}\right) \frac{V_o^{7/3}}{V^{4/3}} + \left(16 - 3B_o^{'}\right) \frac{V_o^{5/3}}{V^{2/3}} \right] + E_o \qquad 6.1$$

Where B_o, $B_o^{'}$ and V_o is the bulk modulus, pressure derivatives and equilibrium volume, respectively. Using B_o, $B_o^{'}$ and V_o from a least square fit of the calculated *V* - *E* curves to equation 6.1, the hydrostatic pressure, P, is established from the *P* – *V* form of the Birch-Murnaghan [112] EOS, which is the volume derivative of the equation. 6.1. The third order Birch-Murnaghan [112] isothermal EOS is given by:

$$P(V) = \frac{3}{2} B_o \left[\left(\frac{V_o}{V} \right)^{7/3} - \frac{5}{3} \left(\frac{V_o}{V} \right)^{5/3} \right] \left\{ 1 + \frac{3}{4} (B_o^{'} - 4) \left[\left(\frac{V_o}{V} \right)^{2/3} - 1 \right] \right\} \qquad 6.2$$

6.1 Tantalum Oxynitrides (TaON)

Tantalum nitride (TaN) is a hard material due to the strong hybridization of the nonmetal 2p orbitals with the metal d orbitals [41]. TaN is commonly found and is chemical inert, corrosion resistant and a hard material [89,114,115]. Tantalum oxide is widely used in electronics as a gate dielectric and in optical devices due to its high transparency and high dielectric constant. A combination of beneficial properties of Ta nitride and Ta oxide results in a material tantalum oxynitrides with variable composition and functionality [116]. TaON is a new material that has not received

much consideration as a potentially hard material. TaON is an oxynitrides material displaying very similar characteristics to ZrO_2 in that it is also has an ambient monoclinic phase [117]. There is a suggestion that cotunnite TaON may have several properties superior to ZrO_2 [118,119] and could be formed from a modest high-pressure treatment of the ambient monoclinic structure. Again there is strong evidence suggesting that phases of TaON could be harder than ZrO_2. Cubic ZrO_2 is notably valued for its hardness and tetragonal ZrO_2 is used as a metastable phase often employed in a composite with other ceramics [4]. The cotunnite phase have recently attracted the attention of researchers and, in particular, can be quenched to ambient conditions and has been suggested as a candidate for a useful superhard material [101]. It is well known, that the high temperature phases of zirconia can be stabilized by introducing the dopants such as CaO, MgO or Y_2O_3 [120]. The ionicity decreases from the monoclinic to cotunnite phase and it is accepted that the larger the ionicity, the lower the hardness of materials [121].

The crystal structures of all the materials considered follow that found in ZrO_2 [4, 121] namely: monoclinic, cubic, tetragonal and orthorhombic. The crystal structures of these phases are shown in fig 1(a)-1(d). All the phases of materials considered are schematically the same. The values of equilibrium (P=0) lattice constant are presented in Table 1. The Birch-Murnaghan equation of state (EOS) was used to fit the energy-volume results, and from this an estimate can be made of bulk moduli B and pressure

derivatives B´ for various phases of TaON. The results are summarized in Table 2. The calculated Birch-Murnaghan equation of state (EOS) for each of the ambient structure are shown in Figs 2 (a) and 2 (b), for TaON in the LDA and GGA respectively. The cubic, tetragonal and cotunnite structures are energetically unstable with respect to the monoclinic phase. The cotunnite phase of TaON has the highest bulk modulus. These phase typically exhibit very high bulk moduli and thus are candidates for hard materials. Theoretical total energies are all given relative to the monoclinic phase, which is the lowest energy phase of all materials considered. In all case it can be seen that the LDA predicts smaller cell volumes than the GGA. To the contrary the bulk moduli for the GGA are smaller than the LDA. The important point is that the calculated results show that various phases lie quite close in energy.

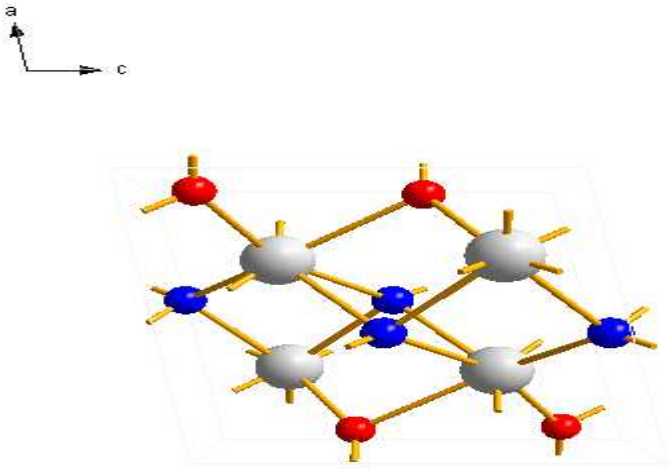

FIG 1(a): Crystal structure of baddeylite Metal oxynitrides LDA

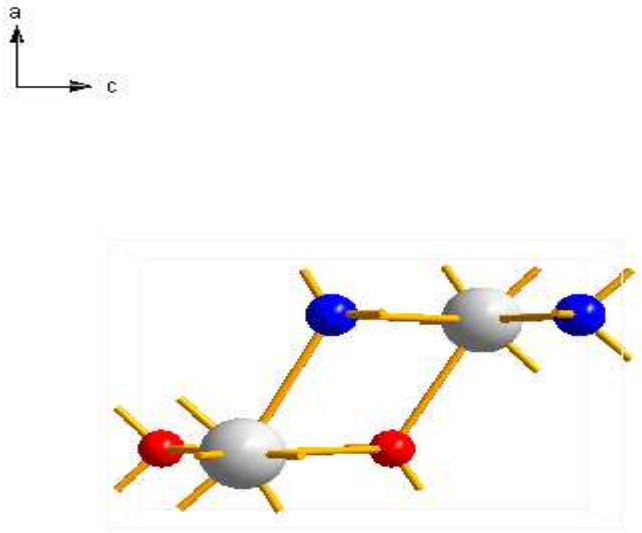

FIG 1 (b): Crystal structure of tetragonal metal oxynitrides LDA

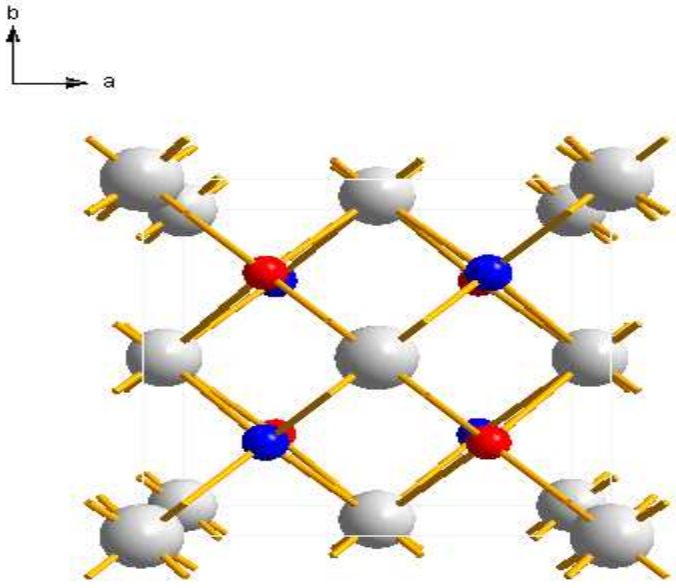

FIG 1 (c): Crystal structure of cubic metal oxynitrides LDA

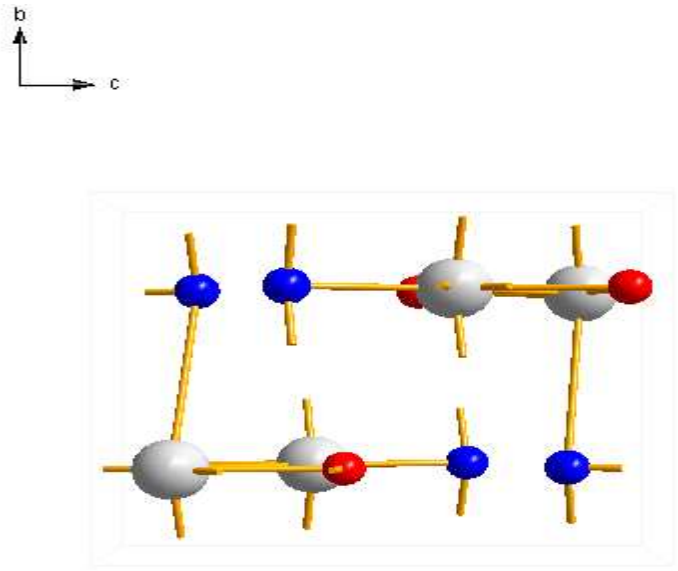

FIG 1 (d): Crystal structure of cotunnite metal oxynitrides LDA

In figs 2 (a) and 2 (b) are plots of the energy against volume for all the phases we have considered. Total energy calculations allow one to decide the stability of the system. Generally, the system with lower energy is said to be the stable one. The monoclinic phase has the lowest equilibrium energy, indicating its stability than the other phases. Thus suggest that the monoclinic phase may be the preferred phase at low pressure. The bulk modulus (B) of cotunnite phase with the space group *Pnma* for TaON was determined to be 369 GPa in the LDA. This B is well compared to 367 GPa of superhard cubic BN [12]. Thus TaON with cotunnite structure may be a superhard

material. So far there is few if any experimental and theoretical work to compare. The calculated bulk modulus (253 GPa) in GGA of TaON in the baddeylite structure is compared very well with a previous theoretical value of 278 GPa [87]. For fluorite structure, the computed bulk (299 GPa) in GGA is in excellent agreement with those of previous theoretical work (299 GPa) [86]. The lattice parameters a, b, and c computed with LDA and GGA methods are within 2, 25% of the experiment [133] for baddeylite structure. For the cotunnite, fluorite, and tetragonal phases, no experimental data on their structure is available; the structure computed here for the cotunnite, fluorite, and tetragonal phases is in reasonable agreement with previous theoretical studies [4].

The relative energies of the phase give some indication of the potential ordering of expected structures at a specific volume. Calculated parameters of possible structures of TaON are shown in Table 2, where the energies are expressed relative to the baddeylite ambient phase. For the LDA the energetic order of the phase found is $E^{baddey} < E^{cot} < E^{tetra} < E^{cubic}$ and for the GGA the energetic ordering sequence is $E^{baddey} < E^{tetra} < E^{cot} < E^{cubic}$.

Figure 3 (a) and 3 (b) gives a free energy – pressure variation with the pressure calculated from the slope of the energy-volume equation of state. The enthalpy difference ΔH is a good measure to compare the relative stability of solid state structures under pressure, because their entropy differences that contribute to the free

enthalpy ΔG are typically small. The baddeylite structure is the most stable modification of TaON up to a pressure at approximately 30 GPa within LDA. Similarly our results with GGA show that baddeylite is more stable up to a pressure at approximately 60 GPa. Above this pressure it will transform into the cotunnite phase. At no point between 0 and 80 GPa is either the tetragonal or fluorite phase predicted to be the most stable form, although the fluorite form is more stable than the tetragonal structure.

Table 1: Crystals structure of metal TaON. GGA results are in brackets. All angles are 90˚ except monoclinic "baddeylite" β

Phase	Space group	Lattice constant		
		a(Å)	b(Å), β	c(Å)
Baddeylite	*$P2_1/c$*	4.999 (5.071)	4.918(5.010)β=99.89˚(99.74˚)	5.140 (5.227)
	Prev theor[81]	4.9878	5.0569 β=99.50	5.2063
	Expt[133]	4.9581	5.0267 β=99.64	5.1752
Cubic	*F43m*	4.827 (4.995)	4.827 (4.995)	4.827 (4.995)
	Prev theor[299]	4.99	4.99	4.98
Tetragonal	*P42/mc*	3.476 (3.528)	3.476 (3.528)	5.101 (5.302)
Cotunnite	*Pnma*	3.198 (3.139)	5.610 (5.470)	6.683 (6.547)

Table 2: Calculated equation of state properties and relative energies of some phases for TaON. GGA results are in brackets.

Phase	Space group	E_{tot} (ev/atom)	V_{eq} ($Å^3$)	B (GPa)	B′
Baddeylite	$P2_1/c$	0.000	11.04 (10.91)	281 (253)	4.67 (5.89)
Cubic	*F43m*	0.409 (0.347)	9.96 (10.40)	335 (299)	4.03 (4.31)
Tetragonal	*P42/mc*	0.249 (0.237)	10.31 (11.01)	253 (204)	5.00 (5.15)
Cotunnite	*Pnma*	0.117 (0.257)	8.91 (9.37)	369 (297)	5.17 (6.62)

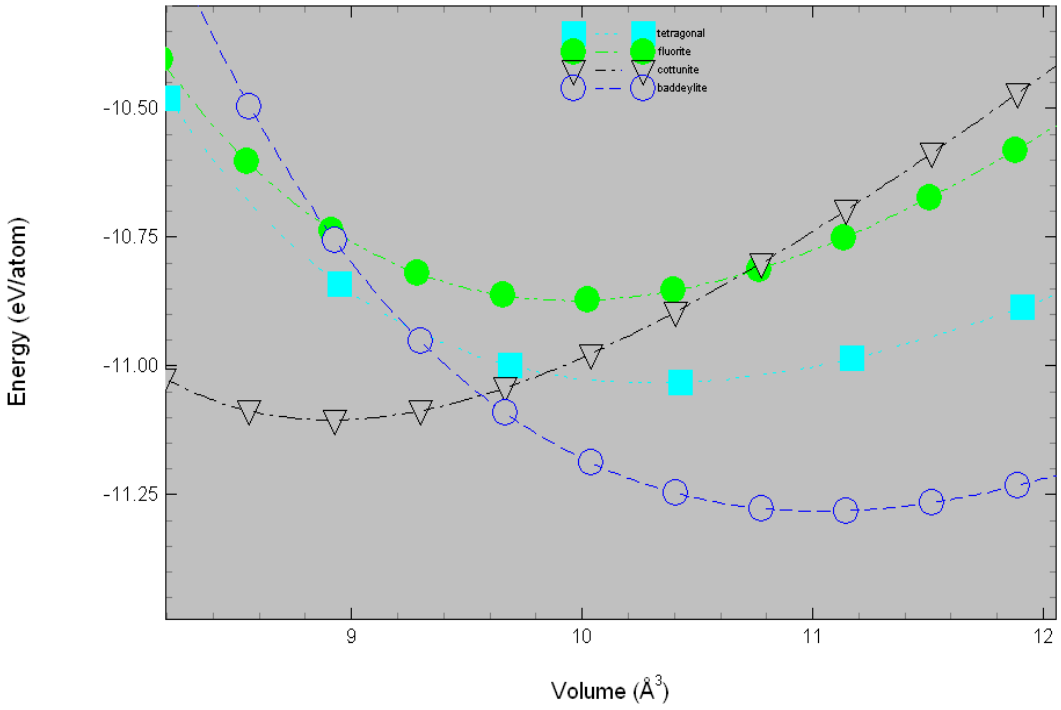

FIG 2 (a): The total energy versus volume for baddeylite, tetragonal, fluorite, and cotunnite structures of TaON calculated with VASP within LDA.

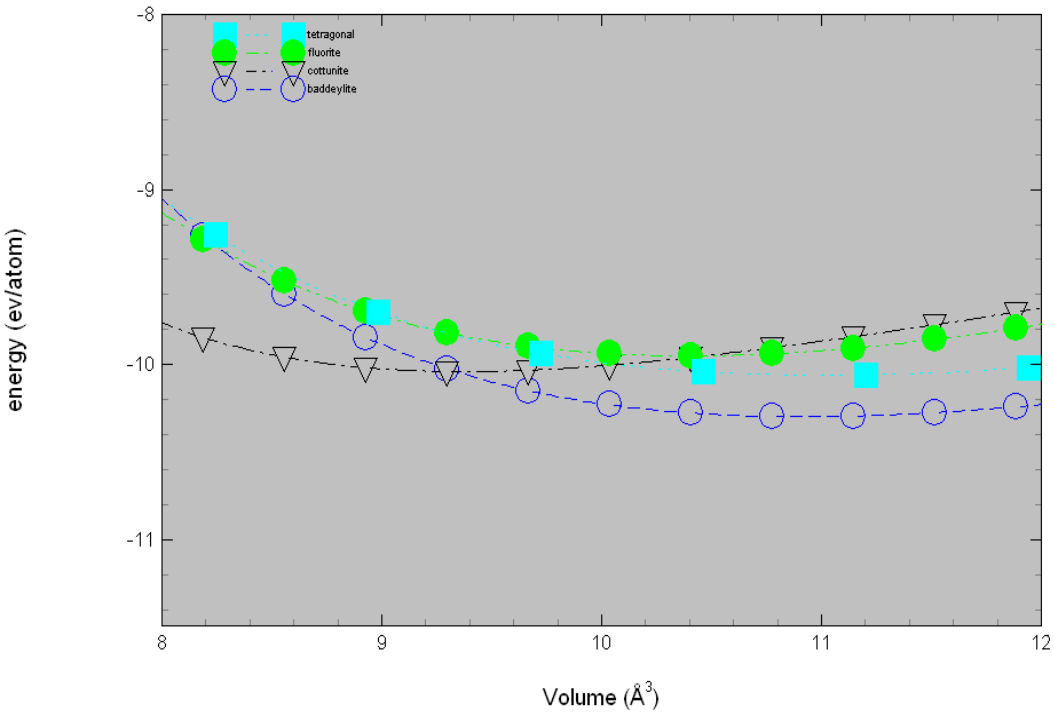

FIG 2 (b): The total energy versus volume for baddeylite, tetragonal, fluorite, and cotunnite structure of TaON calculated with VASP within GGA.

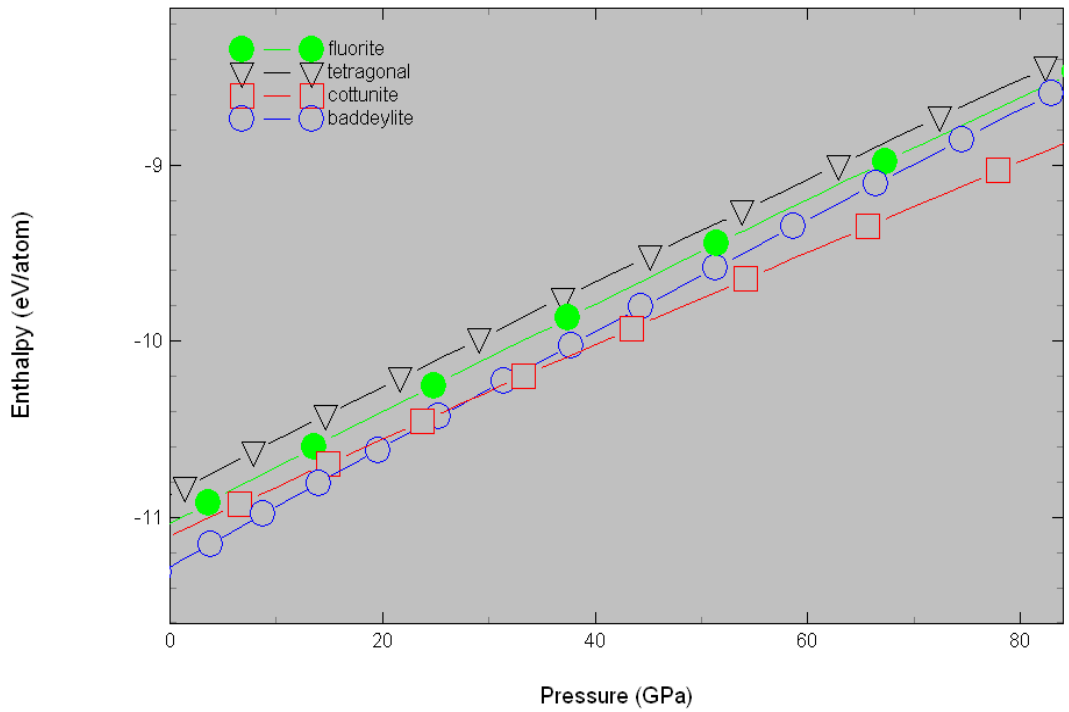

FIG 3 (a): Transition pressure of the various phases as calculated from Birch-Murnaghan equation of state for TaON within LDA.

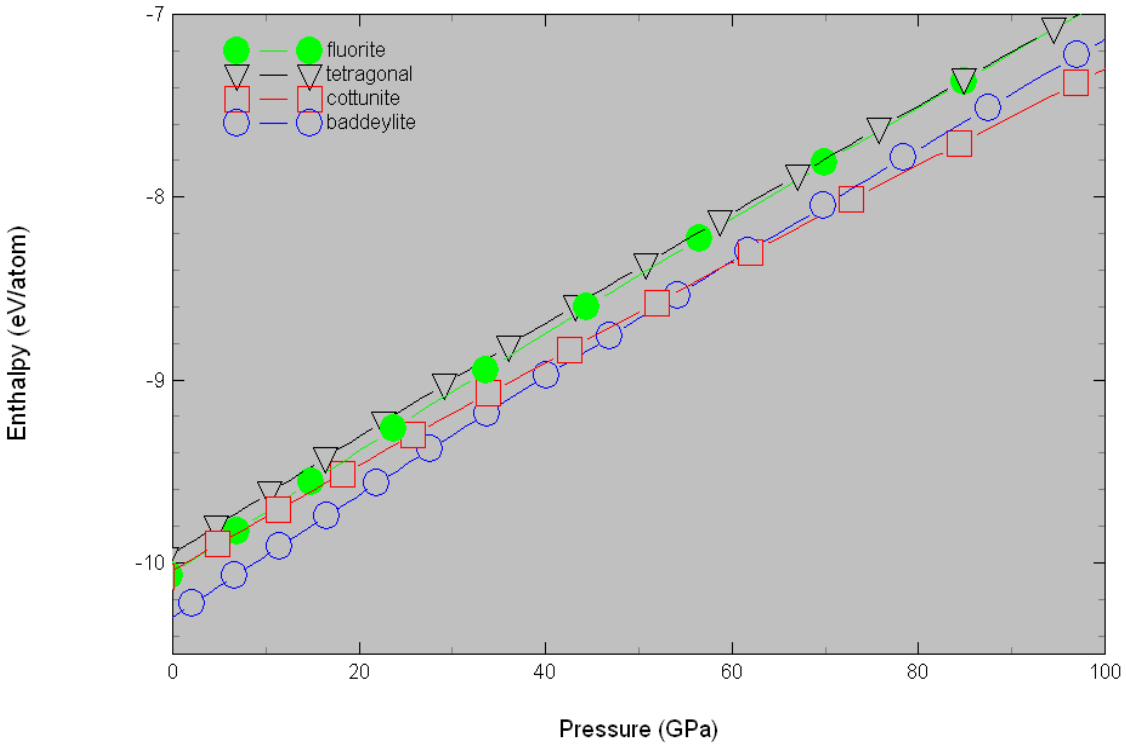

FIG 3 (b): Transition pressure of the various phases as calculated from Birch-Murnaghan equation of state for TaON within GGA.

6.2 Niobium oxynitrides (NbON)

Of the other oxynitrides niobium oxynitrides are another series of new ternary materials [114] that have not so far received much consideration as a potentially hard material. NbON as with TaON crystallize in the ambient phase in the baddeylite structure [122], which is also a high-temperature polymorph of ZrO_2. The central metal atom experiences seven-fold coordination and strictly ordered anion arrangement within this type. The coordination polyhedron in the oxynitrides is formed by the oxygen and four nitrogen atoms. TaON and NbON are anticipated to be similar in that Ta and Nb belong to the same column in the periodic table. NbON is also predicted to exhibit almost the same high pressure behavior as TaON. Major difference between TaON and NbON is that TaON predicted to be semiconductor where as NbON is predicted to be metallic [118]. NbO is metallic, NbO_2 and sub stoichiometric Nb_2O_5 are semiconductors. Preparation of niobium oxynitride at temperature above 900 K was reported [123] and a poor activity of NbN_xO_y in quinoline HDN was observed [124].Kim *et al* [123] studied the synthesis of niobium oxynitrides by reaction between ammonia and niobium pentoxide. The nitridation process was optimized and several different aspects that could influence the reaction were studied. The influence of the crystallographic structure of the precursor oxide on the characteristics

of the oxynitride, the composition of the gaseous mixture, the final temperature of nitridation, as well as the influence of a promoter additive (niobium oxynitrides, itself) on the nitridation process, were all aspects considered in that study. Oyama deals with the aspect of synthesis of NbON [125]. Two metallic phases have been observed in the NbON system; face centered cubic (fcc) structure type and tetragonally deformed NaCL structure [126].

The LDA values of bulk modulus are systematically larger than the GGA values, possibly due to a smaller value of V_o for the former functional. The LDA gives larger energies and bulk moduli than the GGA but lower equilibrium unit-cell volumes. The calculated lattice parameters on NbON in the baddeylite structure match very well with the experimental and the theoretical one calculated by ref [127] and references therein. The results are shown in Table 3. Experimentally NbON is described as a blue-colored semiconductor. Energetic ordering is $E^{baddey} < E^{cot} < E^{tetra} < E^{cubic}$ and $E^{baddey} < E^{tetra} < E^{cot} < E^{cubic}$, for LDA and GGA respectively. Even in the NbON the tetragonal and cubic phases remains metastable throughout the enthalpy-pressure phase diagram fig 5 (a) and 5 (b). The transition pressure from the ground state structure is approximately 30 GPa and 50 GPa for LDA and GGA, respectively.

Table 1 Table 3: Crystals structure of metal NbON. GGA results are in brackets. All angles are 90˚ except monoclinic "baddeylite" β

Phase	Space group	Lattice constant		
		a(Å)	b(Å),β˚	c(Å)
Baddeylite	*P21/c*	5.029 (5.098)	4.956(5.045)β=100.04 (99.85)	5.177 (5.264)
	Prev theor [127]	5.026	5.077 β=100.07	5.243
	Expt[127]	4.970	5.033 β=100.23	5.193
Cubic	*F43m0*	4.954 (5.027)	4.954 (5.027)	4.954 (5.027)
Tetragonal	*P42/mc*	3.517 (3.550)	3.517 (3.550)	5.076 (5.322)
Cotunnite	*Pnma*	3.100 (3.165)	5.441 (5.491)	6.475 (6.602)

Table 2 Table 4: Calculated equation of state properties and relative energies of some phases for NbON. GGA results are in brackets.

Phase	Space group	E_{tot}(V/atom)	V_{eq}(Å^3)	B (GPa)	B´
Baddeylite	*$P2_1/c$*	0.000	10.63(11.13)	266 (221)	4.60 (6.62)
Cubic	*F43m*	0.300(0.343)	10.19 10.60)	304 (275)	4.33 (4.38)
Tetragonal	*P42/mc*	0.205(0.199)	10.52(11.19)	241 (194)	5.01 (5.08)
Cotunnite	*Pnma*	0.130(0.229)	9.13 (9.57)	352 (256)	4.42 (7.74)

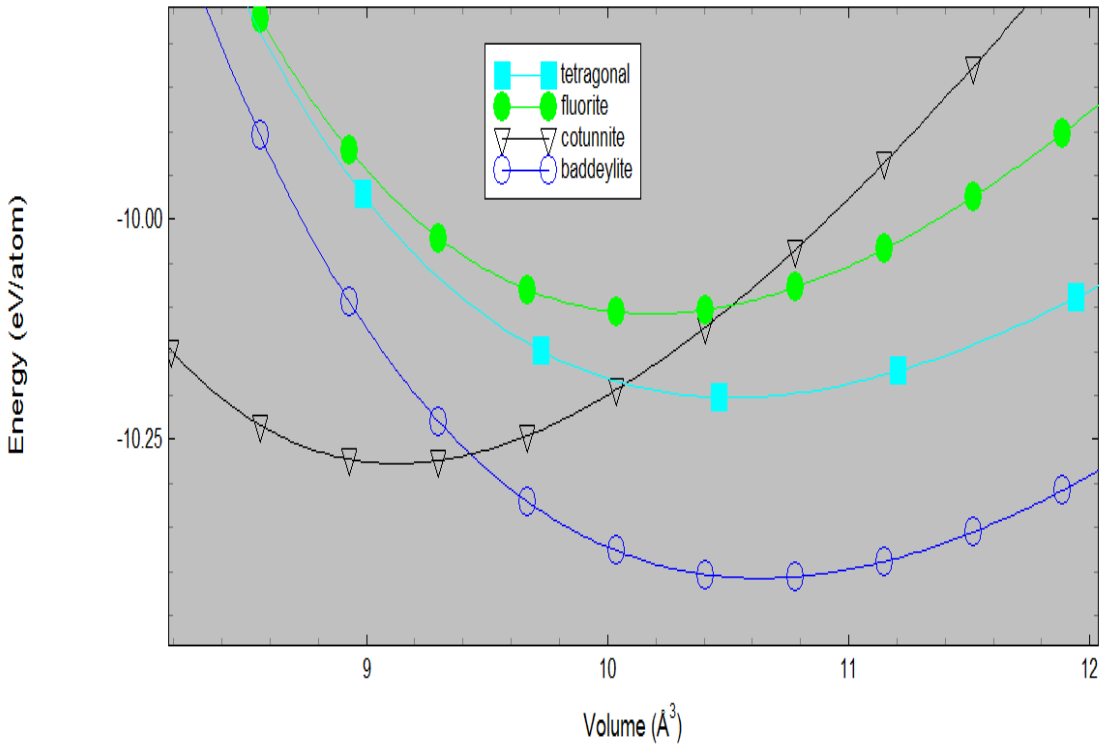

FIG 4 (a): The total energy versus volume for baddeylite, tetragonal, fluorite, and cotunnite structure of NbON calculated with VASP within LDA.

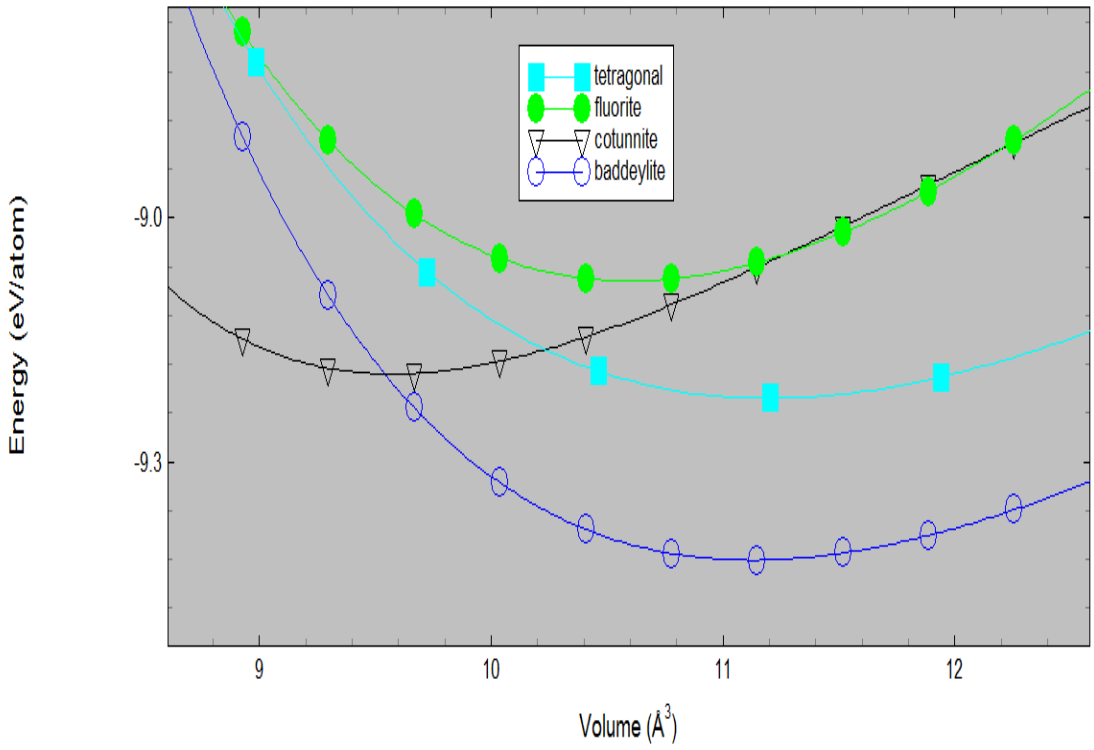

FIG 4 (b): The total energy versus volume for baddeylite, tetragonal, fluorite, and cotunnite structure of NbON calculated with VASP within GGA.

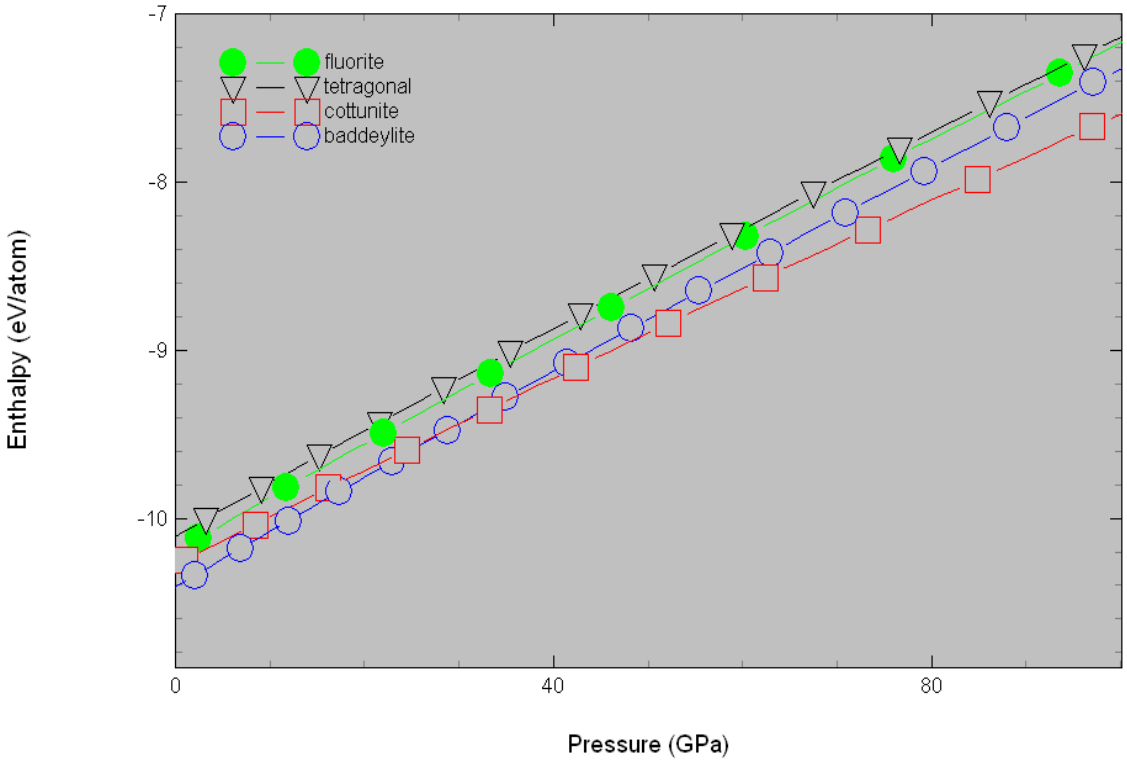

FIG 5 (a): Transition pressure of the various phases as calculated from Birch-Murnaghan equation of state for NbON within LDA.

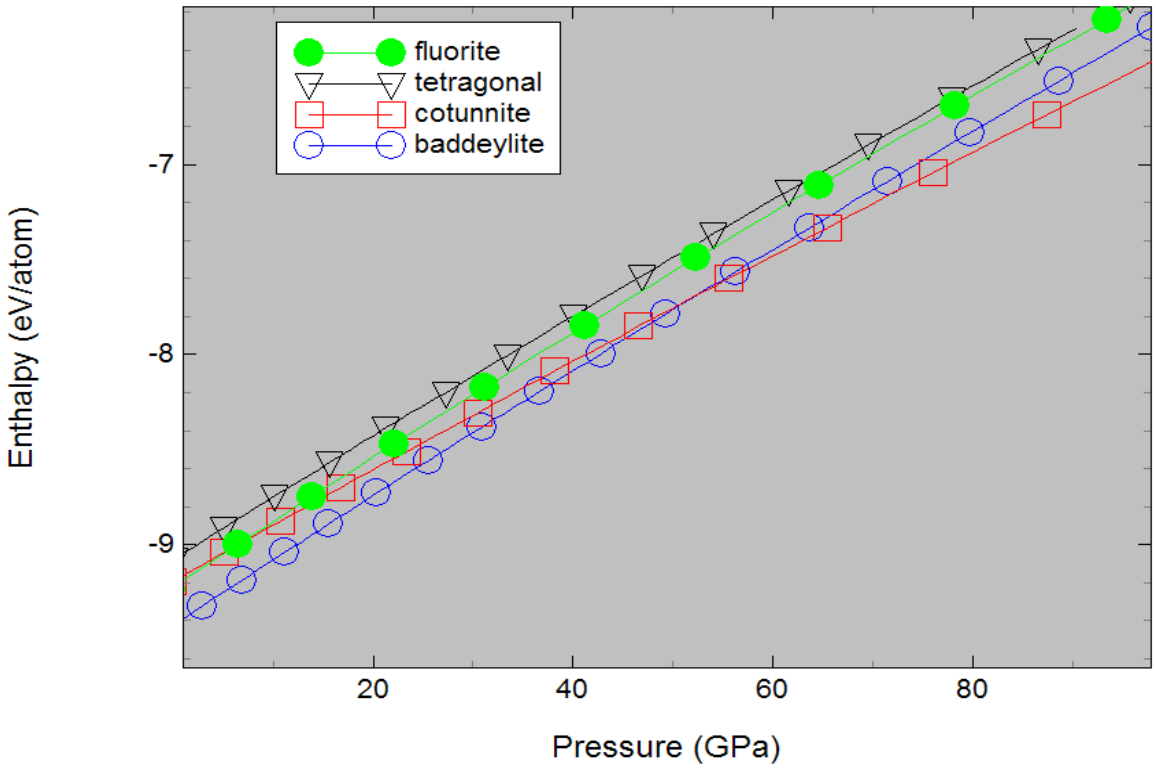

FIG 5 (b): Transition pressure of the various phases as calculated from Birch-Murnaghan equation of state for NbON within GGA.

6.3 Tungsten oxynitrides (WON)

Tungsten is an important of refractory metal due to its high melting temperature and high hardness and is also considered as another candidate for high-temperature and high hardness application. Tungsten oxide, WO_3 is a wide band n-type semiconductor that is very insulating as long as the material is stoichiometric where as tungsten nitride (WN) has a metallic character [128]. Tungsten nitrides (WN) have the following characteristics high melting point, high hardness, chemical inertness and good thermal stability. It is used as diffusion barriers in the microelectronics and electrodes in semiconductor devices [129]. So far there is no much theoretical information about WON as potentially hard material even though there are wide applications of tungsten oxynitride, for example rare earth-WO_xN_y materials are promising as novel colored pigments, with in addition, the possibility to tune the absorption edge to a precise value [130], the films of these oxynitrides may be used for decorative coatings and also interesting for electronic devices such as sensors in thermal radiation detectors [129].

Table 5: Crystals structure of metal WON. GGA results are in brackets. All angles are 90˚ except monoclinic "baddeylite" β

Phase	Space group	Lattice constant		
		A(Å)	b(Å), β	c(Å)
Baddeylite	$P2_1/c$	4.783 (4.856)	4.932(5.022)β=103.44(103.26)	5.179(5.245)
Cubic	*F43m*	4.857 (4.934)	4.857 (4.934)	4.857 (4.934)
Tetragonal	$P4_2/mc$	3.442 (3.460)	3.442 (3.460)	4.982 (5.546)
Cotunnite	*Pnma*	2.829 (2.866)	6.095 (6.325)	6.354 (6.442)

Table 6: Calculated equation of state properties and relative energies for some phases for WON. GGA results are in brackets.

Phase	Space group	E_{tot} (eV/atom)	V_{eq} (Å^3)	B (GPa)	B´
Baddeylite	$P2_1/c$	0.000	9.91 (10.38)	329 (288)	4.13 (4.43)
Cubic	*F43m*	0.421(0.435)	9.55 (10.02)	363 (317)	4.38 (4.43)
Tetragonal	$P4_2/mc$	0.372(0.342)	9.85 (11.08)	276 (162)	6.21 (5.03)
Cotunnite	*Pnma*	0.366(0.384)	9.13 (9.74)	286 (214)	5.60 (6.72)

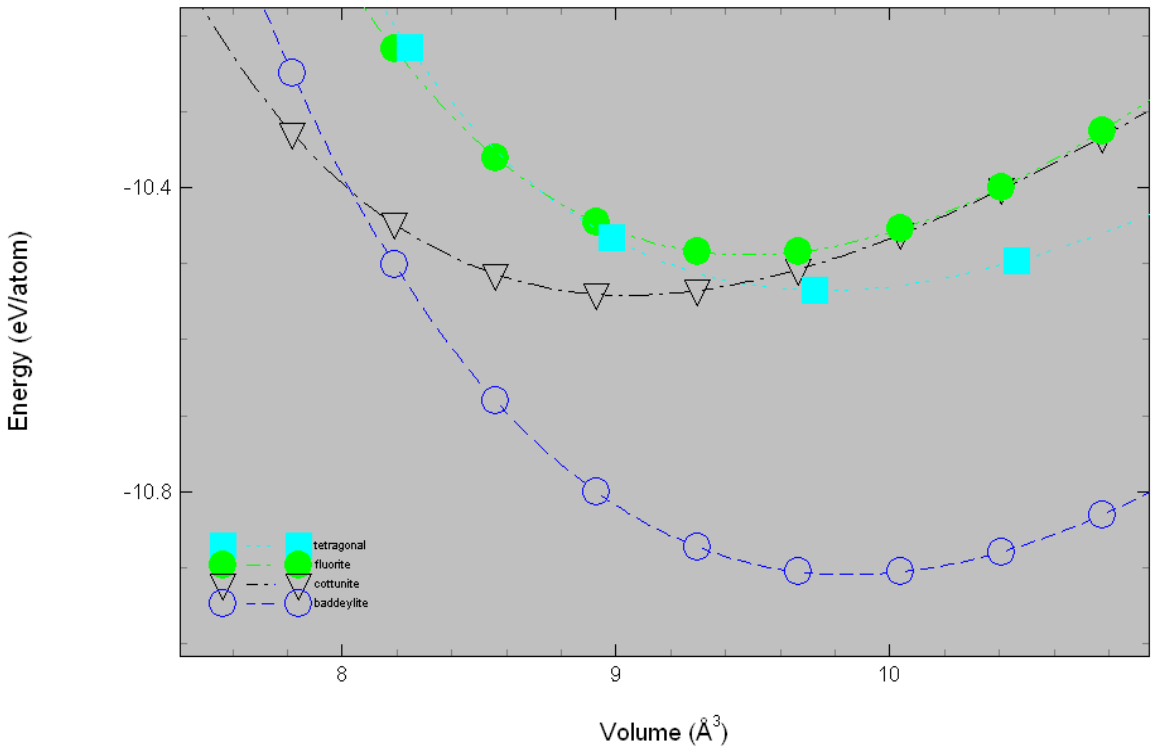

FIG 6 (a): The total energy versus volume for baddeylite, tetragonal, fluorite, and cotunnite structure of WON calculated with VASP within LDA.

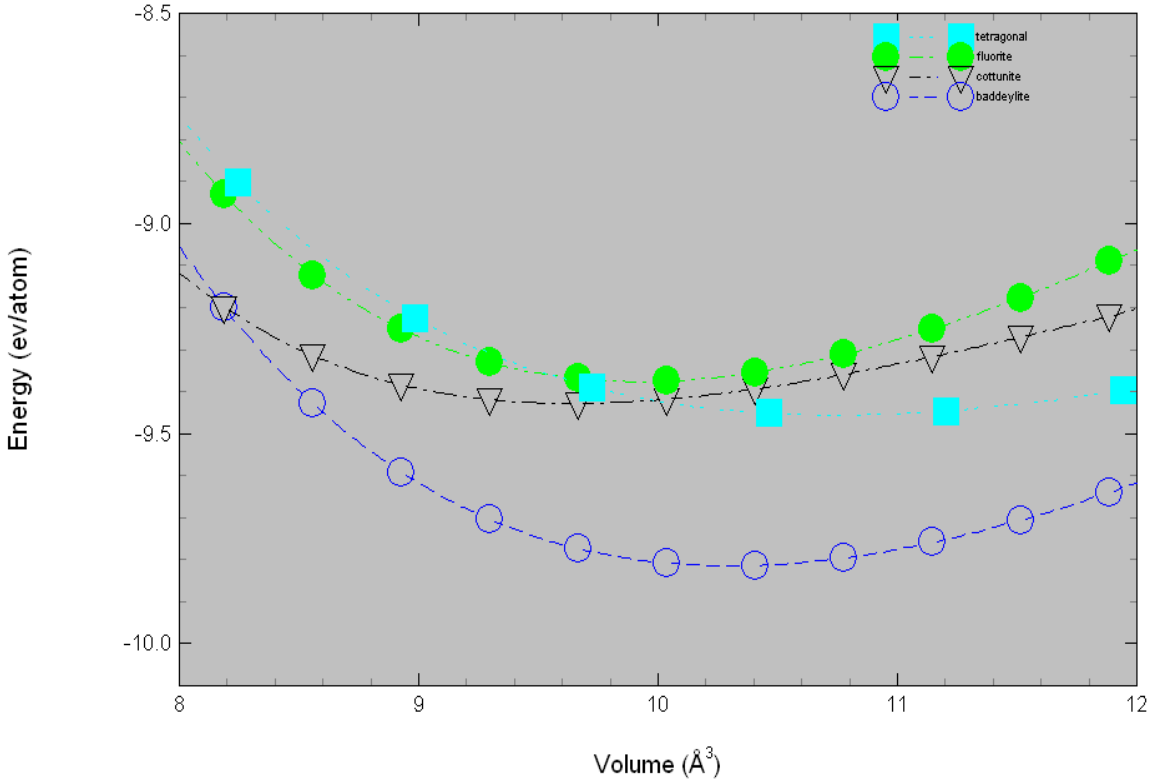

FIG 6 (b): The total energy versus volume for baddeylite, tetragonal, fluorite, and cotunnite structure of WON calculated with VASP within GGA.

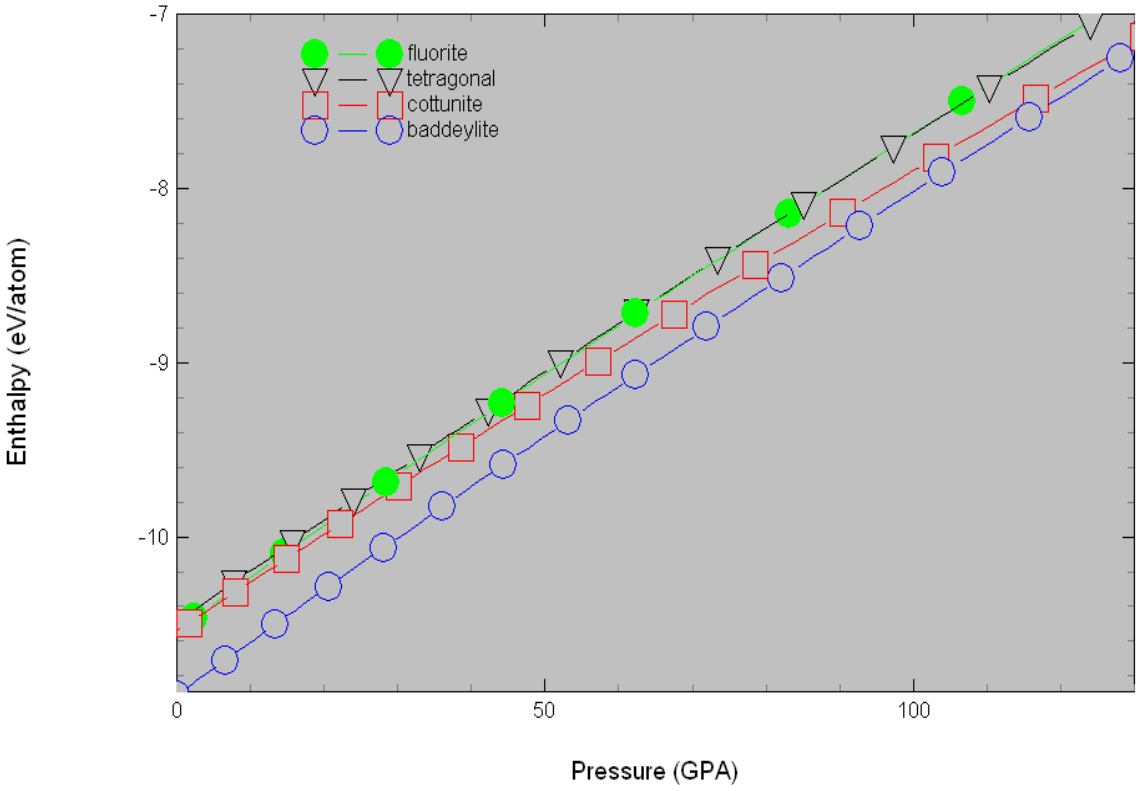

FIG 7 (a): Transition pressure of the various phases as calculated from Birch-Murnaghan equation of state for WON within LDA.

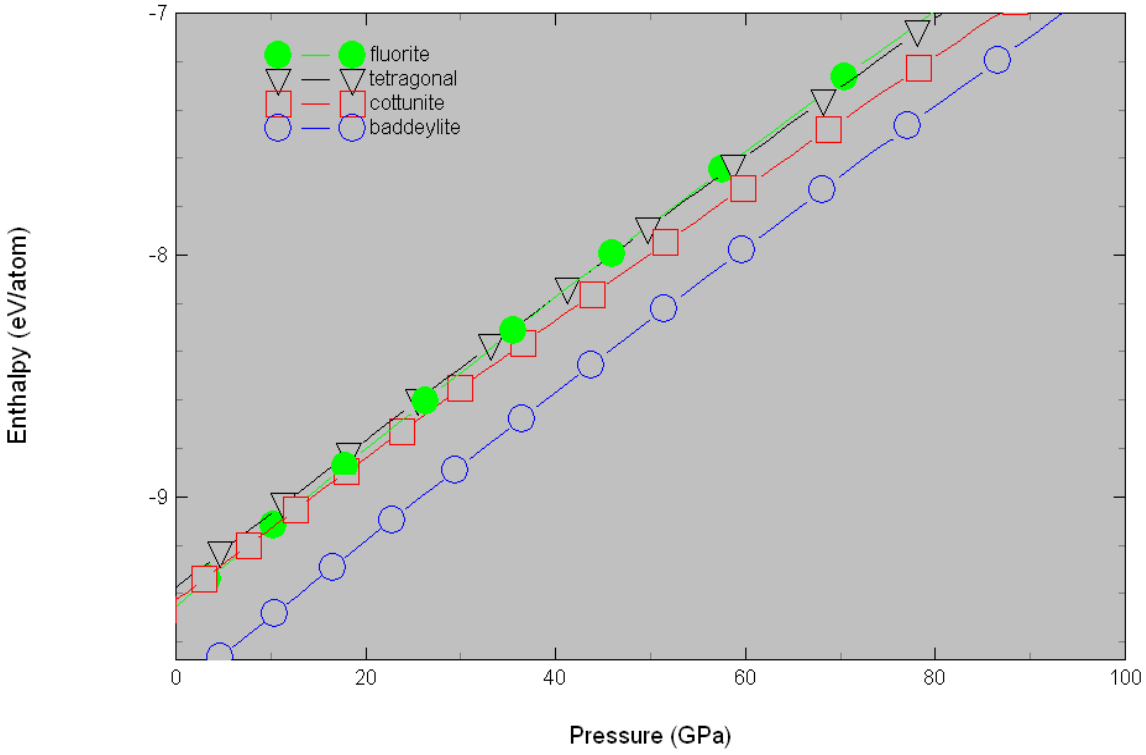

FIG 7 (b): Transition pressure of the various phases as calculated from Birch-Murnaghan equation of state for WON within GGA.

The values of the equilibrium lattice constant calculated are reported in Table 6 and the bulk moduli together with their relative energies are presented in Table 7. As usual, the LDA approach gives larger bulk modulus than the GGA. Bulk modulus (volume stiffness) is sometimes correlated to hardness, especially for cubic materials. Somewhat surprisingly the fluorite phase of WON is promising as new superhard materials as it appear to have high bulk modulus of about 363 GPa which also approaches that of c-BN 367 GPA [12] and is probably associated with the large ionic radius of W. Therefore our prediction indicates that WON in cubic structure is likely to be one of the hardest phases than other considered phases. The total energy versus volume curves are obtained from Birch-Murnaghan EOS fittings. The fact that all considered materials are energetically more stable in the baddeylite structure than any other structure considered is evident in Fig 10. The energetic ordering is $E^{baddey} < E^{cot} < E^{tetra} < E^{cubic}$ and $E^{baddey} < E^{tetra} < E^{cot} < E^{cubic}$, for LDA and GGA respectively.

Fig 6 (a) and 6 (b) for the E-V diagrams can be transformed easily to yield enthalpy vs. pressure diagrams (H-p) fig 7 (a) and 7 (b): the pressure p can be extracted from the E-V graph by a simple numerical differentiation: $p = -\partial E / \partial V$. The enthalpy H is calculated via H = E + pV where E stands for the total energy. The derived relative

enthalpy is a reliable indicator for the stability of a structure type with respect to the applied pressure. In particular baddeylite structure is predicted to be the ground state structure of WON for both LDA and GGA. We find no further modification of WON become more favorable up to 80 GPa and 100 GPa for GGA and LDA respectively. It is also noted that whereas TiON, TaON and NbON behave quantitatively the same, WON is much different in behavior.

6.4 Titanium oxynitrides (TiON)

Titanium compounds have been studied for along time both theoretically and experimentally due to their wide range of many outstanding industrial applications. They can be metals, semiconductors, or ionic insulators depending upon the Ti valence state. Among them, TiN, TiC, and TiO with rocksalt structure, exhibit extremely high hardness, high melting, and chemical stability, are referred to as refractory compounds. Ching [131] reported electronic structure calculations of the spinel phase of c-Ti_3N_4 and c-$SiTi_2N_4$, show that these are highly covalent superhard materials, where c-Ti_3N_4 is a narrow gap semiconductor and c-$SiTi_2N_4$ is a metal. One of the compounds that have received much attention is TiO_2 in the cotunnite structure since it is identified as the hardest known oxide [25]. TiO_xN_y can serve as diffusion barriers in silicon-on-sapphire integrated circuits [129] and as a decorative coating [132].

The crystals parameters obtained are listed in Table 8. Calculation of the bulk modulus of the monoclinic phase of TiON using LDA and GGA yield a lower value of 199 GPa and 155 GPa respectively, of all the phases of the material tested in this work. The GGA results of the bulk modulus raise some concerns about whether the TiON is really superhard as they are all less than 250 GPa [13]. The results from all the phases are presented in Table 8. The energetic ordering is $E^{baddey} < E^{cot} < E^{tetra} < E^{cubic}$ and $E^{baddey} < E^{tetra} < E^{cot} < E^{cubic}$, for LDA and GGA respectively, whence it was deduced that the monoclinic form is stable whereas the cubic, tetragonal and cotunnite forms are not. The energetic ordering is the same to that obtained in other materials.

As can be seen from Table 8, our results predict baddeylite TiON structure to be energetically favoured over the cubic, tetragonal and cotunnite structures. Thus baddeylite is more stable than all other considered phases at zero temperature. However, there is only a very small energy difference between the phases, baddeylite being only 0.076 eV/atom and 0.149 eV/atom more stable than cotunnite for both LDA and GGA respectively. All the TiON phases are extremely close in energy. Fig 8 (a) and 8 (b) shows that the energies of the phases of all the materials considered lie quite close to each other in energy. Actually, these phases are seen to lie within a very close in energy range of each other. This closeness in energy suggests that the transformation between these phases will be quite sensitive and easily affected by, among other factors, temperature and remnant lattice

stresses. There is no experimental result for comparison which warrants further experimental study in this direction.

Table 7: Crystals structure of metal TiON. GGA results are in brackets. All angles are 90˚ except monoclinic "baddeylite" β

Phase	Space group	Lattice constant		
		A(Å)	b(Å),β	c(Å)
Baddeylite	$P2_1/c$	4.768(4.945)	5.056(5.133)β=95.75(95.83)	4.760(4.845)
Cubic	*F43m*	4.799 (4.489)	4.799 (4.894)	4.799 (4.894)
Tetragonal	$P4_2/mc$	3.572 (3.625)	3.572 (3.625)	4.353 (4.509)
Cotunnite	*Pnma*	2.892 (2.934)	5.381 (5.488)	6.366 (6.581)

Table 8: Calculated equation of state properties and relative energies of some phases for TiON. GGA results are in brackets.

Phase	Space group	E_{tot} (eV/atom)	V_{eq} (Å^3)	B (GPa)	B´
Baddeylite	*$P2_1/c$*	0.000	9.53(10.13)	195 (155)	3.75 (4.59)
Cubic	*F43m*	0.203 (0.273)	9.21 (9.77)	267 (228)	4.21 (4.27)
Tetragonal	*$P4_2/mc$*	0.118 (0.125)	9.88 (9.26)	249 (207)	4.28 (4.32)
Cotunnite	*Pnma*	0.076 (0.149)	8.26 (8.84)	279 (216)	5.11 (5.63)

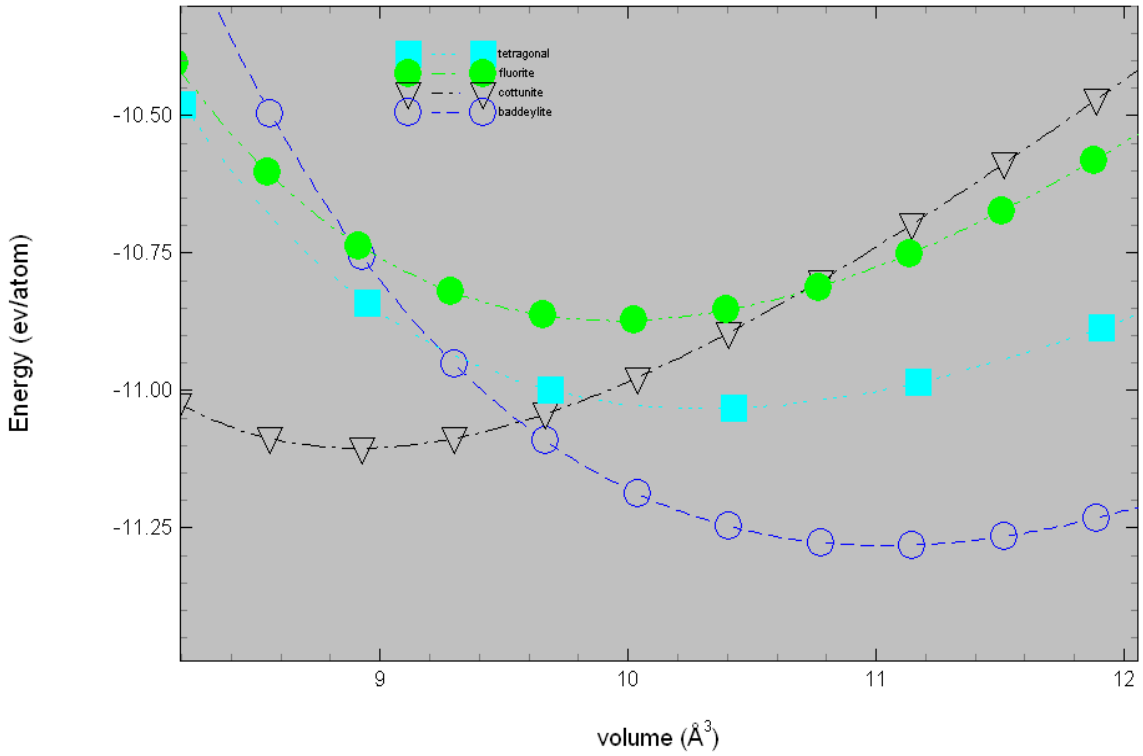

FIG 8 (a): The total energy versus volume for baddeylite, tetragonal, fluorite, and cotunnite structure of TiON calculated with VASP within LDA.

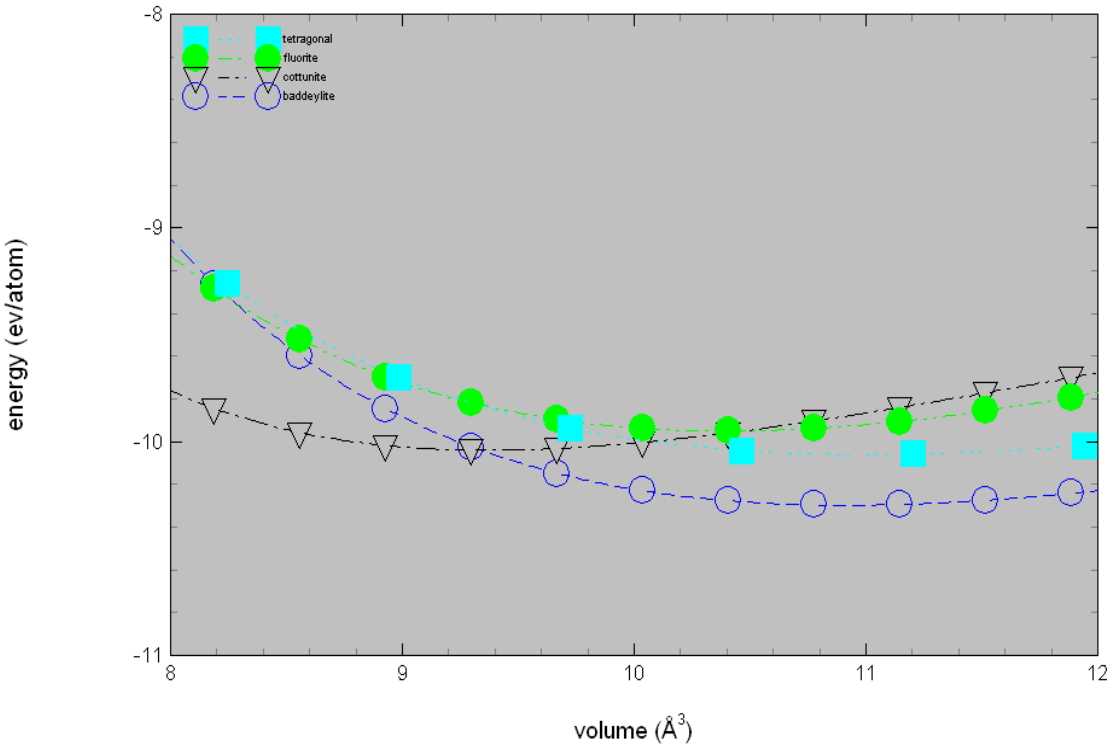

FIG 8 (b): The total energy versus volume for baddeylite, tetragonal, fluorite, and cotunnite structure of TiON calculated with VASP within GGA.

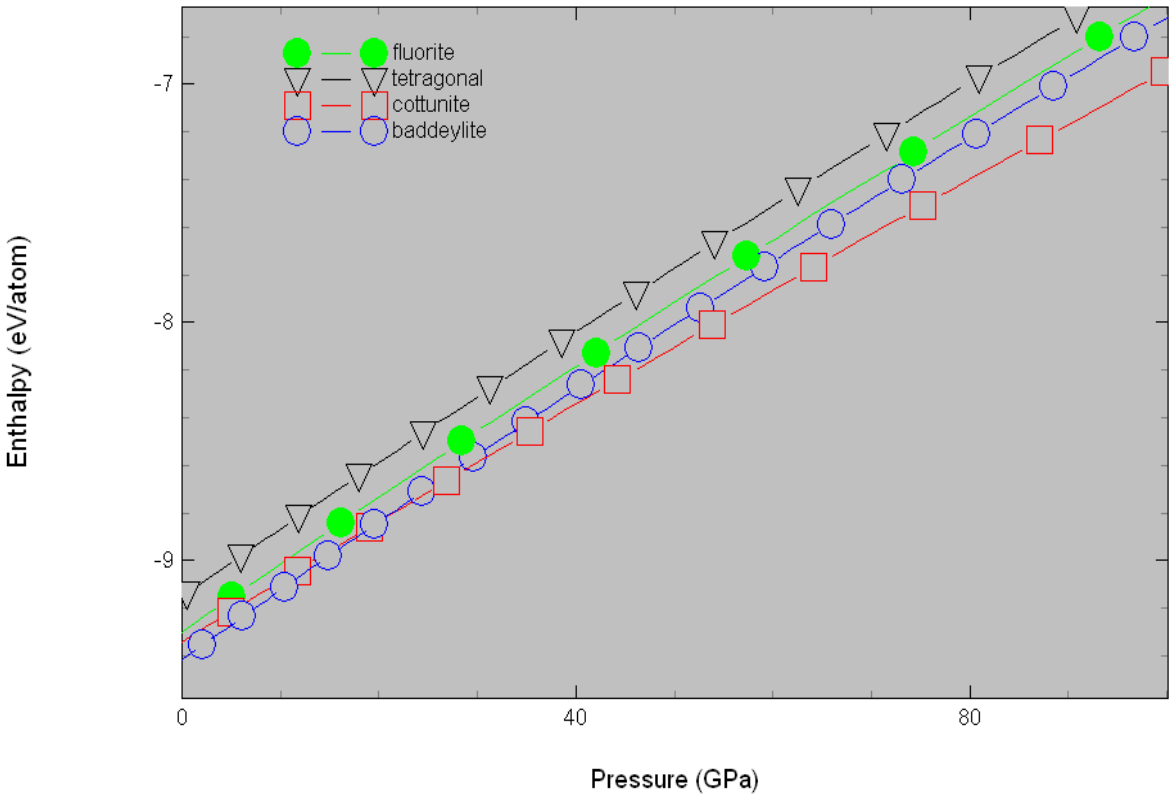

FIG 9 (a): Transition pressure of the various phases as calculated from Birch-Murnaghan equation of state for TiON within LDA.

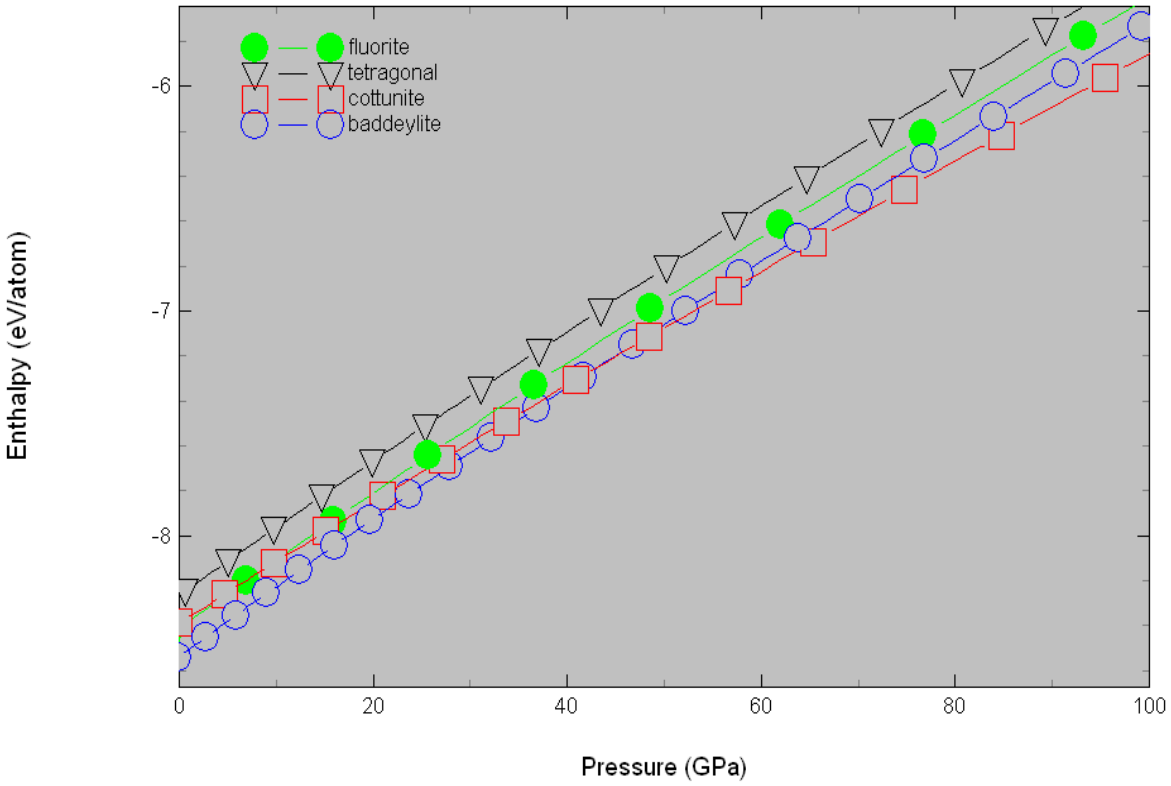

FIG 9 (b): Transition pressure of the various phases as calculated from Birch-Murnaghan equation of state for TiON within GGA.

6.5 Trends in Bulk Modulus

Of all the materials considered, as seen from fig 10 (a) and 10 (b) the LDA and GGA trends behave the same except for WON in the tetragonal phase were it has bulk modulus of 276 GPa and 162 GPa for LDA and GGA respectively. As evident from this figures, it show that the LDA overestimate bulk modulus whereas the GGA underestimate them.

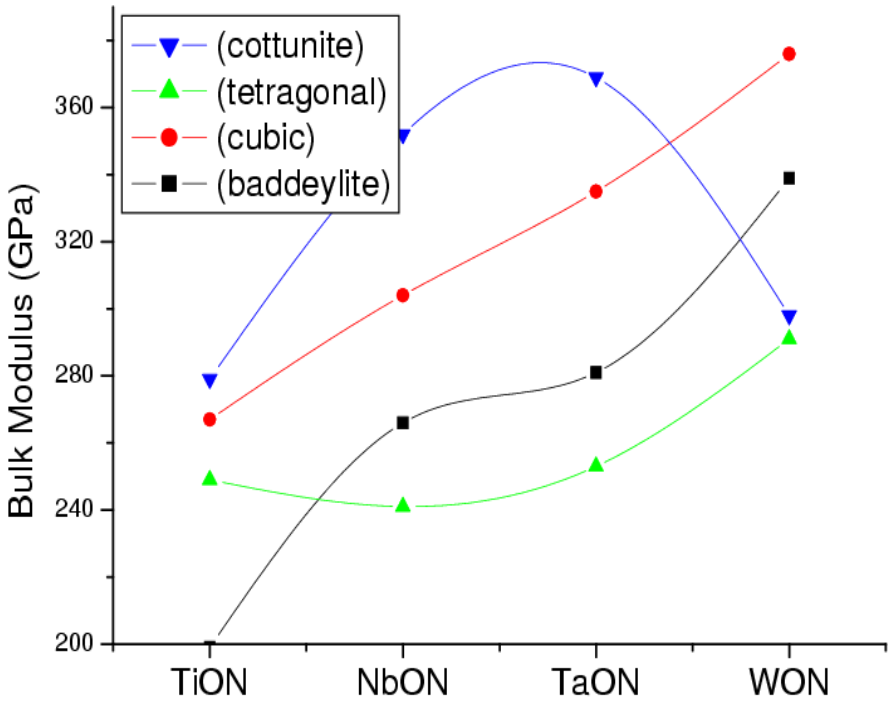

FIG 10 (a): Trends in the bulk modulus of phases of the materials considered for LDAs.

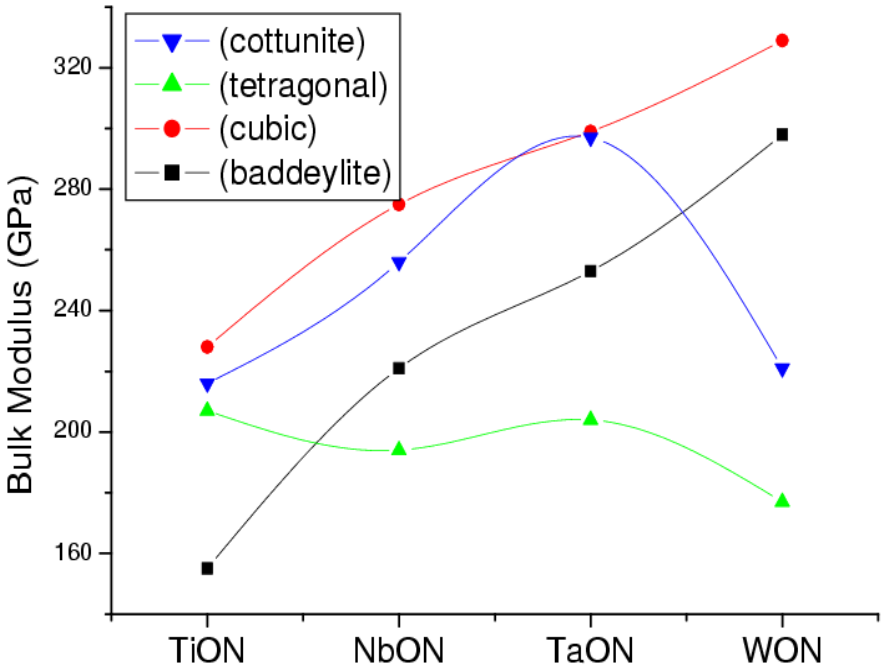

FIG 10 (b): Trends in the bulk modulus of phases of the materials considered for GGAs.

7 Conclusions

In this work the properties of the most important phases of transition metal oxynitrides are investigated. These investigations are performed on a theoretical basis using ab-initio calculations. Of all the materials considered our results predict that the baddeylite structures will be the most stable one. From the calculation considered we can conclude that the baddeylite structure of the materials considered is the ground state at zero pressure while the cotunnite is a high pressure phase. However in all case the transition pressures are seen to be quite high-always being in excess of 20 GPa when starting from the baddeylite structure. We note that beside the GGA bulk modulus values of TiON phases, these phases typically exhibit very high bulk moduli and thus are candidates for hard materials. The numerical data of NbON are slightly different from TaON showing the different atomic nature. The calculated results of TaON and NbON in the baddeylite structure compared very well with the experimental and other theoretical work. In future it will be advisable to study other properties of these materials such as elastic constant. Hopefully this work will assist in how these materials can be synthesized. In all the cases LDA predicts smaller cell volumes than GGA as well as giving bulk moduli that are larger than the GGA. We find large pressures are found to obtain the cotunnite phase for TiON, TaON, and NbON. But several of the phases do appear to have properties superior to ZrO_2. Unlike the phases TiON, TaON,

and NbON, WON behaves quite differently even though we note that WON phase with the fluorite structure has the highest calculated EOS Bulk modulus of 329-375 GPa depending on density functional employed. NbON has a very similar behavior to TaON in chemical, physical and structural properties but the transition pressure to potentially superhard phases probably larger.

The energetic sequence of all the materials considered is the same. The energetic ordering is $E^{baddey} < E^{cot} < E^{tetra} < E^{cubic}$ and $E^{baddey} < E^{tetra} < E^{cot} < E^{cubic}$, for LDA and GGA respectively, whence it was deduced that the monoclinic form is stable whereas the cubic, tetragonal and cotunnite forms are not.

8 References:

1. R. V. Dronskowski, A guide for material scientists, chemists, physicists and others: Computational chemistry of solid state materials, Wiley-VCH, ISBN 3 527 31410 5 (2005)

2. G. Hitoki, T. Tanaka, J. N. Kondo, M. Hara, H. Kobayashi, and K. Domen, Chem. Commun, 1698 (2002)

3. E. Orhan, F. Tessier, and R. Marchand, Solid state sciences **4,** 1071 (2002)

4. J. E. Lowther, Phys. Rev. B **73**, 134110 (2006)

5. W. R. Matizamhuka, M. Herrmann, I. Sigalas, and K. Sempf, J. Am. Ceram. Soc. **90,** 2280 (2007)

6. P. E. Blochl, Phys. Rev. B **50**, 17 953 (1994)

7. D. J. Singh, and L. Nordstrom, Planewaves, Pseudopotentials, and the LAPW Method 2nd edition ISBN 0 387 28780 9 (2006)

8. D. Joubert, Density Functionals Theory and Applications ISBN 3 540 63937 3 (1997)

9. B.R. Wu, C. M. Sung, S. –L. Lee and M. F. Tai, Chinese Journal of Physics Vol. **40**. No. 2, 187 (2002)

10. F. Gao, R. Xu, and K. Liu, Phys. Rev. B **71**, 052103 (2005)

11. F. Gao, J. He, E. Wu, S. Liu, D. Li, S. Zhang, and Y. Tian, Phys. Rev. Lett **91**, 015502 (2003)

12. C. M. Sung, and M. Sung, Materials chem. And phys **43**, 1 (1996)

13. J. E. Lowther, Phys. Stat. Sol. (b) **217**, 533 (2000)

14. J.Haines, J. M. Leger, and G Bocquillon, Annu. Rev. Mater. Res **31,** 1 (2001)

15. P.Bergonzo, F. Foulon, A. Brambilla, D. Tromson, C. Jany, and S. Haan, Diamond & Related materials **9**, 927 (2000)

16. J. –C. Zheng, C. H. A. Huan, A. T. S. Wee, R. –Z. Wang, and Y. –M. Zheng, J. Phys. Condens. Matter **11**, 927 (1999)

17. A. Y. Liu, M. L. Cohen, K. C. Hass, and M. A. Tamor, Phys. Rev. B **43**, 6742 (1991)

18. D. M. Teter, MRS Bull **23**. 22 (1998)

19. G. –M. Rignanese, J. –C. Charlier, and X. Gonze, Phys. Rev. B **66**, 2054416 (2002)

20. D. W. He, Y. S. Zhao, L. Daemen, J. Qian, T. D. Shen, and T. W. Zerda, Appl. Phys. Lett **80**, 643 (2002)

21. Z. C. Pan, H. Sun, and C. F. Chen, Phys. Rev. B **70**, 174115 (2004)

22. K. Benyahia, Z. Nabi, and A. Khalfi, Physica B **339**, 1 (2003)

23. S. Desgrenies, and K. Lagarec, Phys. Rev. B **59**, 8467 (1999)

24. A. Zerr, T. Sekine, J. E. Lowther, W. –Y. Chiang, and I. Tanaka, Advanced Materials, Vol **18,** 2933 (2006)

25. J. M. Leger, J. Haines, M. Schmidt, J. P. Petitet, A. S. Pereira, and J. A. H. da Jornada, Nature. Vol **383**, 401 (1196)

26. L. S. Dubrovovinsky, N. A. Dubrovinskaia, V. Swamy, J. Muscat, N. M. Harrison, R. Ahuja, B. Holm, and B. Johansson, Nature **410**, 653 (2001)

27. H. He, T. Sekeni, T. Kobayashi, and H. Hirosaki, Phys. Rev. B **62**, 11412 (2000)

28. E. Gregoryanz, C. Sanloup, M. Somayazulu, J. Bardo, G. Fiquet, H. –K. Mao, and R. Hemley, Nat. Mater **3**, 294 (2004)

29. E. V. Yakovenko, I. V. Aleksandrov, A. F. Gonchavrov, and S. M. Stishov, Sov. Phys. Jept **68**, 1213 (1989)

30. S. K. R. Patil, S. V. Khare, B. R. Tuttel, J. K. Bording, and S. Kadambaka, Phys. Rev. B **73**, 104118 (2006)

31. B. R. Sahu, and L. Kleinman, Phys. Rev. B **71**, 041101 (R) (2005)

32. H. Cynn, J. E. Klepers, C. S. Yoo, and D. A. Young, Phys. Rev. Lett **88**, 135701 (2002)

33. M. Hebbache, L. Stuparevic, and D. Zivkovic, Solod State Commun **139**, (2006) 227

34. T. Komatsu, M. Nomura, Y. Kakudate, and S. Fujiwara, J. Mater. Chem **6**, 12149 (1996)

35. V. L. Solozhenko, D. Andrault, G. Fiquet, M. Mezouar, and D. C. Rubie, Appl. Phys. Lett **78**, 1385 (2001)

36. E. Knittle, R. B. Kaner, R. Jeanlouz, and M. L. Cohen, Phys. Rev. B **51**, 12149 (1995)

37. S. Chen, X. G. Gong, Phys. Rev. Lett **98**, 015502 (2007)

38. Y. Zhang, H. Sun, and C. Chen, Phys. Rev. Lett **93**, 195504 (2004)

39. V. V. Bzahkin, A. G. Lyapin, and R. J. Hemley, Philos. Mag. A **82**, 231 (2002)

40. P. F Mcmillan, Nature materials **1**, 19 (2002)

41. S. M. Aouadi, J. Appl. Phys **99**, 053507 (2006)

42. M. Hebbache, Solid State Commun **113**, 417 (2000)

43. J. J. Gilman, R. W. Cumberland, and R. B. Kaner, Inter. J. of Refractory metals and Hard materials **24,** 1 (2006)

44. R. M. Martin, Phys. Rev. B **1**, 4005 (1970)

45. F. Gao, Phys. Rev. B **73**, 132104 (2006)

46. C. S. Yan *et al*, Phys. Status. Solid. A **201**, 25 (2004)

47. M. Hebbache, and M. Zemzemi, Phys. Rev. B **70**, 224107 (2004)

48. E. M. Savistkii, editor, handbook of precious metals, English ED editor London Hemisphere publishing corp (1989)

49. C. Wu, Science news Vol. **154,** 28 (1998)

50. S. F. Pugh, Philos. Mag. **45**, 823 (1954)

51. P. Hohenberg, and W. Kohn, Phys. Rev. B **864**, 136 (1964)

52. W. Kohn, and L. J. Sham, Phys. Rev. A **1133**, 140 (1965)

53. L. H. Thomas, Proc. Camb. Phil. Soc **23**, 542 (1927)

54. F. Bloch, Z Physic **57**, 5445 (1929)

55. P. A. M. Dirac, Proc. Camb. Phil. Soc **26**, 376 (1930)

56. D. M. Ceperley, and B. J. Alder, Phys. Rev. Lett **45**, 566 (1980)

57. J. P. Perdew, K. Burke, and M. Ernzerhof, Phys. Rev. Lett **77**, 3865 (1996)

58. J. P. Perdew, K. Burke, and M. Ernzerhof, Phys. Rev. Lett **78**, 1396 (1997)

59. J. P. Perdew, and Y. Wang, Phys. Rev. B **33**, 8800 (1986)

60. J. Perdew, and Y. Wang, Phys. Rev. B **45**, 13244 (1991)

61. E. H. Lieb, and S. Oxford, Int. J. Quantum Chem **19**, 427 (1981)

62. J. Hafner, Acta mater **48**, 71 (2000)

63. E. Hult, Y. Andersson, and B. I. Lundqvist, Phys. Rev. Lett **77**, 2029 (1996)

64. Y. Andersson, D. C. Langreth, and B. I. Lundqvist,Phys. Rev. Lett **76**, 102 (1996)

65. W. Kohn, Y Meir, and D. E. Makarov, Phys. Rev. Lett **80**, 4153 (1998)

66. E. Fermi, Nuovo cimento **11**, 157 (1934)

67. H. J. Hellman, J. Chem. Phys **3**, 61 (1935)

68. J. C. Phillips, and L. Kleinman, Phys. Rev **116**, 287 (1959)

69. W. C. Herring, Phys. Rev **57**, 1169 (1940)

70. C. Audouze, F. Jollet, M. Torrent, and X. Gonze, Phys. Rev. B **73**, 235101 (2006)

71. R. P. Feynman, Phys. Rev. **38**, 340 (1939

72. P. Pulay, Molec. Phys. **17**, 197 (1969)

73. R. Car, and M. Parrinelo, Phys. Rev. Lett. **55**, 2471 (1985)

74. R. M. Martin, Electronic Structure: Basic Theory and Practical Methods, ISBN 0 521 78285 6 (2004)

75. D. R. Hamann, M. Schluter, and C. Chiang, Phys. Rev. Lett **43**, 1494 (1979)

76. D. Vanderbilt, Phys. Rev. B **41**, 7892 (1990)

77. G. Kresse, and D. Joubert, Phys. Rev. B **59**, 1758 (1998)

78. L. Kleinman, and D. M. Bylander, Phys. Rev. Lett **48**, 1425 (1982)

79. S. G. Louie, S. Froyen, and M. L. Cohen. Phys. Rev. B **26**, 1738 (1982)

80. V. Milman, B. Winkler, J. A. White, C. J. Pickard, M. C. Payne, E. V. Akahmatskaya, and R. H. Nobes, Inter. J. Quantum Chem **77**, 895 (2000)

81. M. Valiev, J. H. Weare, J. Phys. Chem. A, Vol**. 103**, 49 (1999)

82. P. Pulay, Chem Phys Lett. **73**, 393 (1980)

83. D. D. Johnson, Phys. Rev. B **38**, 12087 (1988)

84. H. J. Monkhorst, and J. D. Pack, Phys. Rev. B **13**, 5188 (1976)

85. M. Methfessel, and A. T. Paxton, Phys. Rev. B **40**, 3616 (1989)

86. H. Wolff, H. Schilling, M. Lerch, R. Dronskowski, Journal Solid State Chem **179**, 2265 (2006)

87. C. M. Fang, E. Orhan, G. A. de Wijs, H. T. Hontzen, R. A. de Groot, R. Marchand, J. –Y. Saillard, and G. de With, J. Mater. Chem **11**, 1248 (2001)

88. M. Fenker, H. Kappl, O. Banakh, N. Martin. J. F. Pierson, Surface & Coating Tech **201,** 4152 (2006)

89. O. Banakh, C. Csefaivay, P. A. Steiman, M. Fenker, H. Kappl, J. Surface& Coating Tech **200,** 6500 (2006)

90. S. J Clarke, C. W. Michie, and M. J. Rosseinsky, J. Solid State Chem; **146,** 399 (1999)

91. N. Diot, L. Le Gendre, R. Marchand, P. Macaudiere, and P. Maestro, In ISNT II abstract, International Symposium on Nitrides II, ed. S. Hampshire, 1998, Limerick, Ireland, p. 17

92. F. Pors, R. Marchand, Y. Laurent, P. Bacher and G. Roult, Mater. Res. Bull **23**, 1447 (1998)

93. X. Gouin, R. Marchand, Y. Laurent, and F. Gervais, Solid State Commun **93**, 857 (1995)

94. D. Armytage, and B. E. F. Fender, J. Solid State Chem**77**, 67 (1988)

95. K. Stanczyki, H. S. Kim, C. Sayag, D. Brodzki, and G. D-Maradassou, Catalysis Lett **53**, 59 (1998)

96. D. –Hee Cho, T. –Sun Chang, and C. –Ho Shin, Catalysis Lett **67**, 163 (2000)

97. R. Aguiar, D. Logvinovich, A. Weidenkaff, A. Rachel, A. Reller, and S. G. Ebbinghaus, Dyes and Pigments **76**, 70 (2006)

98. R. Pastrana-Fabregas, J. Isasi-Marin, C. Cascales, R. Saez-Puche, Journal of Solid State Chem **180**, (2007) 92

99. J. E. Lowther, J. K. Dewhurst, J. M. Leger, and J. Haines, Phys. Rev. B **60**, 14485 (1999)

100. J. M. Leger, P. E. Tomaszewski, A. Atouf, and A. S. Pereira, Phys. Rev. B **47**, 14075 (1993)

101. J. E. Lowther, MRS Bull **28**, 189 (2003)

102. M. Lerch, F. Krumeich, and R. Hock, Solids State Ionics 95, 87 (1997)

103. J. Wendel, M. Lerch, and W. Laqua, J. Solid State Chem **142**, 163 (1999)

104. J. M. Leger, J. Haines, and B. Lanzat, J. Mat. Sci. Lett **44**, 1688 (1994)

105. B. Silvi, A. Fahmi, C. Minot, and M. Causa, Phys. Rev. B **47**, 11717 (1993)

106. J. E. Lowther, and J. K. Dewhurst, Phys. Rev. B **54**, R 3673 (1996)

107. E. H. _ Bordon, R. Riedel, A. Zerr, P. F. Mcmillan, G. Auffermann, Y. Prots, W. Bronger, R. Kniep, and P. Kroll, Chem. Soc. Rev 35, 987 (2006)

108. N. Diot, R. marchand, J. Haines, J. M. Leger, P. Macaudiere, and S. Hull, J. solid State Chem 1**46**, 390 (1999)

109. W. Y. Ching, S. –Di Mo, I Tanaka, and M Yoshiya, Phys. Rev. B **63**, 064102 (2001)

110. S. Veprek, J. Vac. Science. Tech A **17**, 2401 (1999)

111. F. D. Murnaghan, Proc. Natl. Acad. Sci **30**, 8244 (1944)

112. F. Birch, Phys. Rev **71**, 809 (1947)

113. P. Vinet, J. H. Rose, J. Ferrante, and J.R. Simith, J. Phys. C. **21**, 1941 (1989)

114. J. D Houmes, and H. zur Loye, Journal Of Solid State Chemistry **127**, 267 (1996)

115. M. Kerlau, O. Merdrigranac-Conane, M. Guilloux-Viry, and A. Perrin, Solid States Sciences **6,** 101 (2004)

116. O. Banakh, P.-A. Steinmann, and L Dumitrescu-Buforn, Thin Solid Films **513,** 136 (2006)

117. S. L. Cho, B. S. Kim, H. M. Kim, I. K. Chun, and K. B. Kim, Journal Of The Electrochemical Society **149,** C529 (2002)

118. M. -W. Lumey, and R. Dronskowski, Zeitschrift Fur Anorganische Und Allgemeine Chemie **631,** 887 (2005)

119. J. E. Lowther Phys. Rev. B **72**, 172105 (2005)

120. T. Locherer, L. Dubrovinsky, and H. Fuess, Solid State communications **143**, 408 (2007)

121. J. E. Jaffe, R. A. Bachorz, and M. Gutowski, Phys. Rev. B **72**, 144107 (2005)

122. J. grins, P. O. Kall, and G. Svensson, Journal Of Materials Chemistry **4,** 1293 (1994)

123. H. S. Kim, C. H. Shin, G. Bugli, M. Bureau-Tardy, G. Djega-Mariadassou, Appl. Catal. A. Gen. **119,** 223 (1994)

124. H. S. Kim, C. Sayag, G. Bugli, G. Djega-Mariadassou, M. Boudard, Mtaer. Res. Soc. Symp. Proc **368**, 3 (1995)

125. V. Schwartz, and S. T. Oyama, Chem. Mater **9**, 3052 (1997)

126. N. Schonberg, Acta Chemica Scandinavica **8,** 208 (1954)

127. M. –W Lumey, Quantum- Chemical calculations of Transition- Metal Oxynitrides, Von der Fakultat fur Mathematik, Informatik und Naturwissenschaften der Rheinisch-Westalischen Technischen Hochschule Aachen zur Erlangung des akademischen Grades eines Doktors der Naturwissen schaften genehmigte Dissertation, thesis 2006,

128. F. –B. Wu, S. –K. Tien, J. -G. Duh, and J. –W. Lee, Journal electronic materials **34,** 12 (2005)

129. S. H. Mohamed, and A. Anders, Surface and Coatings Technolgy **201**, 2977 (2006)

130. N. Doit, O. Larcher, R. Marchand, J.Y. Kempf, P. Macaudiere, J. alloys Compd **45**, 323 (2000)

131. W. Y. Ching, S. –D. Mo, L. Ouyang, I. Tanaka, and M. Yoshiya, Phys. Rev. B **61**, 10609 (2000)

132. F. Vaz, P. Cerqueira, L. Rebouta, S.M. C. Nascimento, E. Alves, P. Goudeau, J. P. Riviere, K. Pischow, and J. de Rijk, Thin Solid Films **449**, 447 (2004)

133. D. Armytage, and B. E. F. Fender, Acta cryst, B **70**, 809 (1974)